



Search for new physics in final states with an energetic jet or a hadronically decaying W or Z boson and transverse momentum imbalance at $\sqrt{s} = 13$ TeV

The CMS Collaboration*

Abstract

A search for new physics using events containing an imbalance in transverse momentum and one or more energetic jets arising from initial-state radiation or the hadronic decay of W or Z bosons is presented. A data sample of proton-proton collisions at $\sqrt{s} = 13$ TeV, collected with the CMS detector at the LHC and corresponding to an integrated luminosity of 35.9 fb^{-1} , is used. The observed data are found to be in agreement with the expectation from standard model processes. The results are interpreted as limits on the dark matter production cross section in simplified models with vector, axial-vector, scalar, and pseudoscalar mediators. Interpretations in the context of fermion portal and nonthermal dark matter models are also provided. In addition, the results are interpreted in terms of invisible decays of the Higgs boson and set stringent limits on the fundamental Planck scale in the Arkani-Hamed, Dimopoulos, and Dvali model with large extra spatial dimensions.

Published in Physical Review D as doi:10.1103/PhysRevD.97.092005.

1 Introduction

Several astrophysical observations [1–3] provide compelling evidence for the existence of dark matter (DM), a type of matter not accounted for in the standard model (SM). To date only gravitational interactions of DM have been observed and it remains unknown if DM has a particle origin and could interact with ordinary matter via SM processes. However, many theoretical models have been proposed in which DM and SM particles interact with sufficient strength that DM may be directly produced with observable rates in high energy collisions at the CERN LHC. While the DM particles would remain undetected, they may recoil with large transverse momentum (p_T) against other detectable particles resulting in an overall visible p_T imbalance in a collision event. This type of event topology is rarely produced in SM processes and therefore enables a highly sensitive search for DM. Similar event topologies are predicted by other extensions of the SM, such as the Arkani-Hamed, Dimopoulos, and Dvali (ADD) model [4–8] of large extra spatial dimensions (EDs).

This paper describes a search for new physics resulting in final states with one or more energetic jets and an imbalance in p_T due to undetected particles. The jets are the result of the fragmentation and hadronization of quarks or gluons, which may be produced directly in the hard scattering process as initial-state radiation or as the decay products of a vector boson V (W or Z). These final states are commonly referred to as ‘monojet’ and ‘mono- V ’. Several searches have been performed at the LHC using the monojet and mono- V channels [9–15]. This analysis makes use of a data sample of proton-proton (pp) collisions at $\sqrt{s} = 13$ TeV collected with the CMS detector at the LHC, corresponding to an integrated luminosity of 35.9 fb^{-1} . This sample is approximately three times larger than the one used in Ref. [14]. The analysis strategy is similar to that of previous CMS searches, and simultaneously employs event categories to target both the monojet and mono- V final states. In an improvement compared to previous searches, in this paper revised theoretical predictions and uncertainties for γ +jets, Z +jets, and W +jets processes based on recommendations of Ref. [16] are used. In addition to interpretations in the context of simplified DM models [17–19], in this paper the results are further studied in the context of the fermion portal (FP) dark matter model [20], the light nonthermal DM model [21, 22], and the ADD model.

In many simplified DM models, DM particles are assumed to be Dirac fermions that interact with SM particles through a spin-1 or spin-0 mediator [18, 20, 23–38]. These interactions are classified into four different types, depending on whether the mediator is a vector, axial-vector, scalar, or pseudoscalar particle. The spin-0 mediators are assumed to couple to the SM particles via Yukawa couplings. The SM Higgs boson is a specific example of a scalar mediator that may couple to the DM particles. Combined results of the direct searches for invisible Higgs bosons have been presented by both the ATLAS and CMS Collaborations, which respectively obtain observed upper limits of 0.25 and 0.24 on the Higgs boson invisible branching fraction, $\mathcal{B}(H \rightarrow \text{inv.})$, at 95% confidence level (CL) [39, 40].

In the FP dark matter model [20], the DM particle, assumed to be either a Dirac or Majorana fermion, couples to a color-triplet scalar mediator (ϕ_u) and an SM fermion. In the investigated model, the DM candidate is assumed to couple only to up-type quarks, with a coupling strength parameter $\lambda_u = 1$. In this model, the mediators couple to quarks and the DM candidate, and may be singly produced in association with a DM particle. This associated production yields a monojet signature, while pair production of mediators can be observed in multijet final states with significant p_T imbalance, as shown in Fig. 1.

The light nonthermal DM model [21, 22] is a minimal extension of the SM where the DM particle is a Majorana fermion (χ_{DM}) that interacts with the up-type quarks via a colored scalar

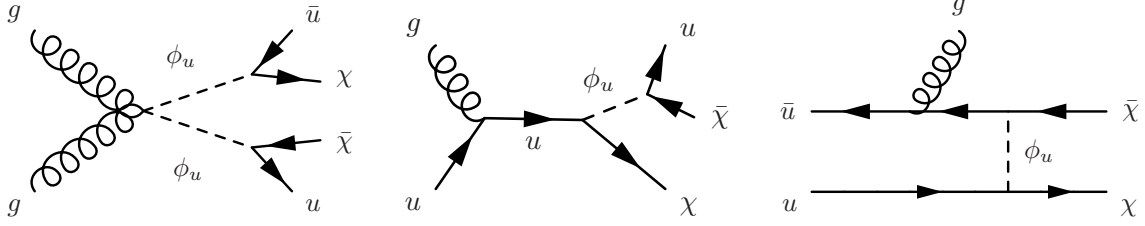


Figure 1: Examples of Feynman diagrams of the main production mechanisms at the LHC of DM particles in association with a quark or gluon in the fermion portal model providing multijet (left) and monojet (middle, right) signatures.

mediator (X_1) with a coupling strength parameter λ_2 . This new colored mediator also interacts with the down-type quarks with a coupling strength parameter λ_1 . Baryon number is not conserved in interactions of such mediators, and therefore the nonthermal DM model could explain both the baryon abundance and the DM content of the universe. The DM particle mass in this model must be nearly degenerate with the proton mass to ensure the stability of both the proton and the DM particle. Thus, the latter can be singly produced at the LHC, as shown in Fig. 2. This leads to a final state that includes large p_T imbalance and an energetic jet, whose p_T distribution is a Jacobian peak at half the X_1 mass.

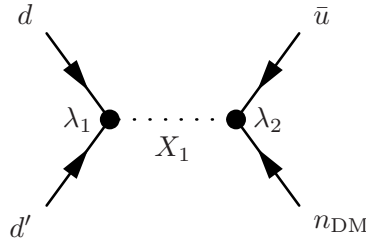


Figure 2: Example of Feynman diagram of the main production mechanism at the LHC of DM particles in the nonthermal model resulting in the monojet final state. In this diagram, d and d' represent different down-type quark generations.

The ADD model of EDs offers an explanation of the large difference between the electroweak unification scale and the Planck scale (M_{Pl}), at which gravity becomes as strong as the SM interactions. In the simplest ADD model, a number (n) of EDs are introduced and are compactified on an n -dimensional torus of common radius R . In this framework, the SM particles and their interactions are confined to the ordinary 3+1 space-time dimensions, while gravity is free to propagate through the entire multidimensional space. The strength of the gravitational force in 3+1 dimensions is effectively diluted. The fundamental Planck scale M_D of this 4+ n -dimensional theory is related to the apparent four-dimensional Planck scale according to $M_{\text{Pl}}^2 \approx M_D^{n+2} R^n$. The production of gravitons (G) is expected to be greatly enhanced by the increased phase space available in the EDs. Once produced in proton-proton collisions, the graviton escapes undetected into the EDs and its presence must be inferred from an overall p_T imbalance in the collision event, again leading to a monojet signature, as shown in Fig. 3.

For all models, the signal extraction is performed using the distribution of the p_T imbalance in each event category. In the context of simplified DM models, the results of the search are reported in terms of excluded values of the masses of the mediator and of the DM particles. In the context of the FP and nonthermal DM models, the results of the search are reported in terms of excluded values of the mass of the mediator particle, and either the DM particle mass or the strength of the coupling between the mediator and the DM or SM particles. The case of

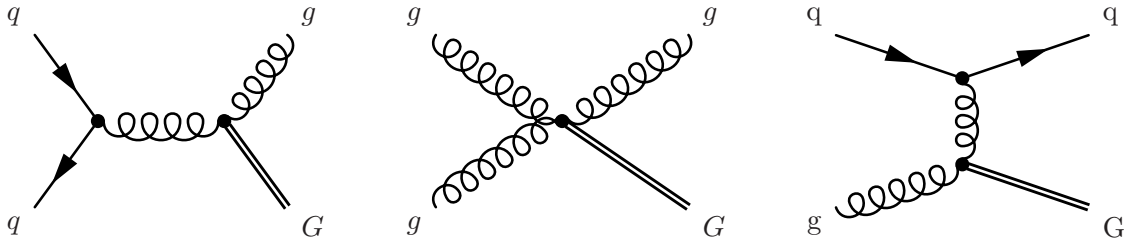


Figure 3: Examples of Feynman diagrams of the main production mechanisms of gravitons at the LHC that provide monojet signatures in the ADD model.

a Higgs boson decaying to invisible (e.g., DM) particles is also considered, and the results are reported in terms of upper limits on the branching fraction to invisible particles of the Higgs boson with a mass of 125 GeV [41–43], assuming SM production cross sections (σ_{SM}). In the ADD model, the results are reported in terms of limits on the fundamental Planck scale as a function of the number of extra spatial dimensions.

This paper is organized as follows. A brief overview of the CMS detector and a description of the event reconstruction is given in Section 2. Information about the event simulation is provided in Section 3 and the event selection is provided in Section 4. Section 5 details the background estimation strategy used in the analysis. Finally, the results of the search are described in Section 6 and summarized in Section 7.

2 The CMS detector and event reconstruction

The central feature of the CMS apparatus is a superconducting solenoid of 6 m internal diameter, providing a magnetic field of 3.8 T. Within the solenoid volume are a silicon pixel and strip tracker, a lead tungstate crystal electromagnetic calorimeter (ECAL), and a brass and scintillator hadron calorimeter (HCAL), each composed of a barrel and two endcap sections. Forward calorimeters extend the pseudorapidity (η) coverage provided by the barrel and endcap detectors. Muons are detected in gas-ionization chambers embedded in the steel flux-return yoke outside the solenoid. A more detailed description of the CMS detector, together with a definition of the coordinate system used and the relevant kinematic variables, can be found in Ref. [44].

The CMS particle-flow (PF) event algorithm [45] reconstructs and identifies each individual particle with an optimized combination of information from the various elements of the detector. The energy of photons is directly obtained from the ECAL measurement, corrected for zero-suppression effects. The energy of muons is obtained from the curvature of the corresponding track. The energy of electrons is determined from a combination of the electron momentum at the primary interaction vertex as determined by the tracker, the energy of the corresponding ECAL cluster, and the energy sum of all bremsstrahlung photons spatially compatible with originating from the electron track. The energy of charged hadrons is determined from a combination of their momentum measured in the tracker and the matching ECAL and HCAL energy deposits, corrected for zero-suppression effects and for the response function of the calorimeters to hadronic showers. Finally, the energy of neutral hadrons is obtained from the corresponding corrected ECAL and HCAL energy.

The missing transverse momentum vector (\vec{p}_T^{miss}) is computed as the negative vector sum of the transverse momenta (\vec{p}_T) of all the PF candidates in an event, and its magnitude is denoted as p_T^{miss} . Hadronic jets are reconstructed by clustering PF candidates using the infrared and

collinear safe anti- k_T algorithm [46]. Jets clustered with distance parameters of 0.4 and 0.8 are referred to as AK4 and AK8 jets, respectively. The reconstructed vertex with the largest value of summed physics-object p_T^2 is taken to be the primary pp interaction vertex. The physics objects are those returned by a jet finding algorithm [46, 47] applied to all charged PF candidates associated with the vertex, plus the corresponding associated p_T^{miss} .

Jet momentum is determined as the vector sum of all particle momenta in the jet, and is found from simulation to be within 5 to 10% of the true momentum over the full p_T spectrum and detector acceptance. An offset correction is applied to jet energies to take into account the contribution from additional proton-proton interactions within the same or nearby bunch crossings (pileup). Jet energy corrections are derived from simulation, and are confirmed with *in situ* measurements of the energy balance in dijet, multijet, γ +jet, and leptonic Z+jet events [48]. Additional selection criteria are applied to each event to remove spurious jet-like features originating from isolated noise patterns in certain HCAL regions. Such corrections and selections are also propagated to the p_T^{miss} calculation [49, 50].

Muons within the geometrical acceptance of $|\eta| < 2.4$ are reconstructed by combining information from the silicon tracker and the muon system [51]. The muons are required to pass a set of quality criteria based on the number of spatial points measured in the tracker and in the muon system, the fit quality of the muon track, and its consistency with the primary vertex of the event. The isolation requirements for muons are based on the sum of the energies of the PF candidates originating from the primary vertex within a cone of $\Delta R < 0.4$ around the muon direction, excluding the muons and electrons from the sum. The muon isolation variable is corrected for pileup effects by subtracting half of the p_T sum of the charged particles that are inside the isolation cone and not associated with the primary vertex. In this paper, ‘loose’ muons are selected with an average efficiency of 98% and are used as a condition to veto the events, whereas ‘tight’ muons are selected with an average efficiency of 95% and are used to tag the events in the control samples.

Electrons within the geometrical acceptance of $|\eta| < 2.5$ are reconstructed by associating tracks reconstructed in the silicon detector with clusters of energy in the ECAL [52]. Well-identified electron candidates are required to satisfy additional identification criteria based on the shower shape of the energy deposit in the ECAL and the consistency of the electron track with the primary vertex [53]. Electron candidates that are identified as coming from photon conversions in the detector material are removed. The isolation requirements are separated from electron identification, and are based on the sum of the energies of the PF candidates originating from the primary vertex within a cone of $\Delta R < 0.3$ around the electron direction, excluding the muons and electrons from the sum. The mean energy deposit in the isolation cone of the electron coming from pileup is estimated following the method described in Ref. [52] and subtracted from the isolation sum. In this paper, ‘loose’ electrons are selected with an average efficiency of 95% and are used as a condition to veto the events, whereas ‘tight’ electrons with an average efficiency of 70% are used to select the events in the control samples.

Photon candidates are reconstructed from energy deposits in the ECAL using algorithms that constrain the clusters to the size and shape expected from a photon [54]. The identification of the candidates is based on shower-shape and isolation variables. For a photon to be considered to be isolated, scalar p_T sums of PF candidates originating from the primary vertex, excluding the muons and electrons within a cone of $\Delta R < 0.3$ around the photon candidate, are required to be below the bounds defined. Only the PF candidates that do not overlap with the electromagnetic shower of the candidate photon are included in the isolation sums. In this paper, ‘loose’ photon candidates are required to be reconstructed within $|\eta| < 2.5$, whereas

‘tight’ photon candidates used are required to be reconstructed in the ECAL barrel ($|\eta| < 1.44$). The tight photon candidates are also required to pass identification and isolation criteria that ensure an efficiency of 80% in selecting prompt photons, and a sample purity of 95% for the control samples.

Hadronically decaying τ lepton candidates detected within $|\eta| < 2.3$ are required to pass identification criteria using the hadron-plus-strips algorithm [55]. The algorithm identifies a jet as a hadronically decaying τ lepton candidate if a subset of the particles assigned to the jet is consistent with the decay products of a τ candidate. In addition, τ candidates are required to be isolated from other activity in the event. The isolation requirement is computed by summing the p_T of the PF charged and PF photon candidates within an isolation cone of $\Delta R = 0.5$ and 0.3 , respectively, around the τ candidate direction. A more detailed description of the isolation requirement can be found in Ref. [55].

3 Simulated samples

To model the SM backgrounds, simulated Monte Carlo (MC) samples are produced for the Z+jets, W+jets, γ +jets, and quantum chromodynamics (QCD) multijet processes at leading order (LO) using the MADGRAPH5_aMC@NLO 2.2.2 [56] generator and are generated with up to four additional partons in the matrix element calculations. The samples for the $t\bar{t}$ and single top quark background processes are produced at next-to-leading order (NLO) using POWHEG 2.0 and 1.0, respectively [57, 58], and the set of diboson (WW, WZ, ZZ) samples is produced at LO with PYTHIA 8.205 [59].

Vector and axial-vector monojet and mono-V dark matter signals are simulated at NLO using the DMSIMP models [60, 61] with the MADGRAPH5_aMC@NLO generator. Both scalar and pseudoscalar monojet and mono-V production contain gluon-initiated loop processes. In the case of mono-V signals, no direct couplings of the mediator to vector bosons are considered. All samples are generated at LO with one additional parton in the matrix element calculations, taking into account finite top quark mass effects and using the MADGRAPH5_aMC@NLO generator in conjunction with the DMSIMP models.

The SM Higgs boson signal events produced through vector boson fusion and gluon fusion are generated using the POWHEG generator [62, 63]; for each sample the cross section is normalized to the next-to-NLO (NNLO) and next-to-NNLO, respectively. The SM Higgs boson production in association with W or Z bosons is simulated at LO using the JHUGENERATOR 5.2.5 generator [64] and normalized to the NNLO cross section.

The ADD ED signal is simulated at LO in QCD using the PYTHIA generator, requiring $\hat{p}_T > 80$ GeV, where \hat{p}_T denotes the transverse momentum of the outgoing parton in the parton-parton center-of-mass frame. The PYTHIA truncation setting is used to suppress the cross section by a factor of M_D^4/\hat{s}^2 for $\hat{s} > M_D^2$, where \hat{s} is the center-of-mass energy of the incoming partons, to ensure validity of the effective field theory.

Lastly, both the FP dark matter signal and the nonthermal DM signal models are simulated at LO using the MADGRAPH5_aMC@NLO generator. In the FP dark matter signal model, the coupling strength parameter is fixed to be $\lambda_u = 1$ while, in the nonthermal DM signal model, the mass of the DM particle is fixed to the proton mass to assure the stability of both the proton and the DM particle. In this latter model, coupling ranges of 0.01–1.5 for λ_1 and 0.01–2.0 for λ_2 are considered, to ensure the mediator width is less than about 30% of its mass.

The MC samples produced using MADGRAPH5_aMC@NLO, POWHEG, and JHUGENERATOR

generators are interfaced with PYTHIA using the CUETP8M1 tune [65] for the fragmentation, hadronization, and underlying event description. In the case of the MADGRAPH5_aMC@NLO samples, jets from the matrix element calculations are matched to the parton shower description following the MLM [66] (FxFx [67]) prescription to match jets from matrix element calculations and parton shower description for LO (NLO) samples. The NNPDF 3.0 [68] parton distribution functions (PDFs) are used in all generated samples. The propagation of all final-state particles through the CMS detector are simulated with GEANT 4 [69]. The simulated events include the effects of pileup, with the multiplicity of reconstructed primary vertices matching that in data. The average number of pileup interactions per proton bunch crossing is found to be 23 for the data sample used in this analysis [70].

4 Event selection

Signal region events are selected using triggers with thresholds of 110 or 120 GeV on both $p_{T,\text{trig}}^{\text{miss}}$ and $H_{T,\text{trig}}^{\text{miss}}$, depending on the data taking period. The $p_{T,\text{trig}}^{\text{miss}}$ corresponds to the magnitude of the vector \vec{p}_T sum of all the PF candidates reconstructed at the trigger level, while the $H_{T,\text{trig}}^{\text{miss}}$ is computed as the magnitude of the vector \vec{p}_T sum of jets with $p_T > 20$ GeV and $|\eta| < 5.0$ reconstructed at the trigger level. The energy fraction attributed to neutral hadrons in these jets is required to be smaller than 0.9. This requirement suppresses anomalous events with jets originating from detector noise. To be able to use the same triggers for selecting events in the muon control samples used for background prediction, muon candidates are not included in the $p_{T,\text{trig}}^{\text{miss}}$ nor $H_{T,\text{trig}}^{\text{miss}}$ computation. The trigger efficiency is measured to be 97% for events passing the analysis selection for $p_T^{\text{miss}} > 250$ GeV and becomes fully efficient for events with $p_T^{\text{miss}} > 350$ GeV.

Candidate events are required to have $p_T^{\text{miss}} > 250$ GeV. In the monojet category, the highest p_T (leading) AK4 jet in the event is required to have $p_T > 100$ GeV and $|\eta| < 2.4$, whereas in the mono-V category, the leading AK8 jet is required to have $p_T > 250$ GeV and $|\eta| < 2.4$. In both categories, the leading jet is also required to have at least 10% of its energy coming from charged particles and less than 80% of its energy attributed to neutral hadrons. This selection helps to remove events originating from beam-induced backgrounds. In addition, the analysis employs various event filters to reduce events with large misreconstructed p_T^{miss} [49] originating from noncollision backgrounds.

The main background processes in this search are the $Z(\nu\nu)+\text{jets}$ and $W(\ell\nu)+\text{jets}$ processes. The $Z(\nu\nu)+\text{jets}$ process is an irreducible background and constitutes the largest background in the search. In contrast, the background from $W(\ell\nu)+\text{jets}$ is suppressed by imposing a veto on events containing one or more loose muons or electrons with $p_T > 10$ GeV, or τ leptons with $p_T > 18$ GeV. Events that contain a loose, isolated photon with $p_T > 15$ GeV and $|\eta| < 2.5$ are also vetoed. This helps to suppress electroweak (EW) backgrounds in which a photon is radiated from the initial state. To reduce the contamination from top quark backgrounds, events are rejected if they contain a b-tagged jet with $p_T > 20$ GeV and $|\eta| < 2.4$. These jets are identified using the combined secondary vertex algorithm (CSVv2) [71, 72], adopting a working point corresponding to correctly identifying a jet originating from a bottom quark with a probability of 80% and misidentifying a jet originating from a charm quark (light-flavor jet) with a probability of 40 (10)%. Lastly, QCD multijet background with E_T^{miss} arising from mismeasurements of the jet momenta is suppressed by requiring the minimum azimuthal angle between the \vec{p}_T^{miss} direction and each of the first four leading jets with p_T greater than 30 GeV to be larger than 0.5 radians.

To select an event in the mono-V category, a leading AK8 jet is identified as a jet arising from hadronic decays of Lorentz-boosted W or Z bosons. Such jets typically have an invariant mass, computed from the momenta of jet's constituents, between 65 and 105 GeV [73]. The mass of the leading AK8 jet is computed after pruning based on the technique [74, 75] involving reclustering the constituents of the jet using the Cambridge–Aachen algorithm [76] and removing the soft and wide-angle contributions to jets in every recombination step. The pruning algorithm is controlled by a soft threshold parameter $z_{\text{cut}} = 0.1$ and an angular separation threshold of $\Delta R > m_{\text{jet}}/p_{\text{T}}^{\text{jet}}$. This technique yields improved jet mass resolution owing to reduced effects coming from the underlying event and pileup. The N -subjettiness variable τ_N [77] is also employed to further isolate jets arising from hadronic decays of W or Z bosons. This observable measures the distribution of jet constituents relative to candidate subjet axes in order to quantify how well the jet can be divided into N subjets. Therefore, the ratio of the ‘2-subjettiness’ to the ‘1-subjettiness’ (τ_2/τ_1) has excellent capability for distinguishing jets originating from boosted vector bosons from jets originating from light quarks and gluons. The pruned jet mass and N -subjettiness requirements, whose use is referred to as V tagging, result in a 70% efficiency for tagging jets originating from V bosons and a 5% probability of misidentifying a jet as a V jet. Events that do not qualify for the mono-V category are assigned to the monojet category. The common selection requirements for both signal categories are summarized in Table 1, while the category-specific selection requirements are reported in Table 2.

Table 1: Summary of the common selection requirements for mono-V and monojet categories.

Variable	Selection	Target background
Muon (electron) veto	$p_{\text{T}} > 10 \text{ GeV}, \eta < 2.4(2.5)$	$Z(\ell\ell)+\text{jets}, W(\ell\nu)+\text{jets}$
τ lepton veto	$p_{\text{T}} > 18 \text{ GeV}, \eta < 2.3$	$Z(\ell\ell)+\text{jets}, W(\ell\nu)+\text{jets}$
Photon veto	$p_{\text{T}} > 15 \text{ GeV}, \eta < 2.5$	$\gamma+\text{jets}$
Bottom jet veto	$\text{CSVv2} < 0.8484, p_{\text{T}} > 15 \text{ GeV}, \eta < 2.4$	Top quark
$p_{\text{T}}^{\text{miss}}$	$> 250 \text{ GeV}$	QCD, top quark, $Z(\ell\ell)+\text{jets}$
$\Delta\phi(\vec{p}_{\text{T}}^{\text{jet}}, \vec{p}_{\text{T}}^{\text{miss}})$	$> 0.5 \text{ radians}$	QCD
Leading AK4 jet p_{T} and η	$> 100 \text{ GeV}$ and $ \eta < 2.4$	All

Table 2: Summary of the selection requirements for the mono-V category. Events that fail the mono-V selection are assigned to the monojet category.

Leading AK8 jet	Mono-V selection
p_{T} and η	$> 250 \text{ GeV}$ and $ \eta < 2.4$
τ_2/τ_1	< 0.6
Mass (m_{jet})	$65 < m_{\text{jet}} < 105 \text{ GeV}$

5 Background estimation

The largest background contributions, from $Z(\nu\nu)+\text{jets}$ and $W(\ell\nu)+\text{jets}$ processes, are estimated using data from five mutually exclusive control samples selected from dimuon, dielectron, single-muon, single-electron, and $\gamma+\text{jets}$ final states as explained below. The hadronic recoil p_{T} is used as a proxy for $p_{\text{T}}^{\text{miss}}$ in these control samples, and is defined by excluding identified leptons or photons from the $p_{\text{T}}^{\text{miss}}$ calculation.

5.1 Control sample selection

Dimuon and single-muon control sample events are selected using full signal region criteria with the exception of the muon veto. Events in the dimuon control sample are selected requiring leading (subleading) muon p_T greater than 20 (10) GeV and an invariant mass in the range 60 to 120 GeV, compatible with a Z boson decay. Events are vetoed if there is an additional loose muon or electron with $p_T > 10$ GeV. In the single-muon control sample, exactly one tightly identified, isolated muon with $p_T > 20$ GeV is required. No additional loose muons or electrons with $p_T > 10$ GeV are allowed. In addition, the transverse mass (M_T) of the muon- \vec{p}_T^{miss} system is required to be less than 160 GeV and is computed as $M_T = \sqrt{2p_T^{\text{miss}}p_T^\mu(1 - \cos\Delta\phi)}$, where p_T^μ is the p_T of the muon, and $\Delta\phi$ is the angle between \vec{p}_T^μ and \vec{p}_T^{miss} .

Dielectron and single-electron control sample events are selected with an isolated single-electron trigger with a p_T threshold of 27 GeV. In boosted Z(ee)+jets events, the two electrons produced in the decay typically have so little separation such that their tracks are included in each other's isolation cones. Therefore, to recover efficiency in selecting high- p_T Z candidates at the trigger level, a nonisolated single-electron trigger with a p_T threshold of 105 GeV is used. Events in the dielectron control sample are required to contain exactly two oppositely charged electrons with leading (trailing) electron p_T greater than 40 (10) GeV. Similar to the dimuon control sample case, the invariant mass of the dielectron system is required to be between 60 and 120 GeV to be consistent with a Z boson decay. The events in the single-electron control sample are required to contain exactly one tightly identified and isolated electron with $p_T > 40$ GeV. In addition, the contamination from QCD multijet events in this control sample is suppressed by requiring $p_T^{\text{miss}} > 50$ GeV and $M_T < 160$ GeV.

Lastly, the γ +jets control sample is selected using events with one high- p_T photon collected using single-photon triggers with p_T thresholds of 165 or 175 GeV, depending on the data taking conditions. The photon is required to have $p_T > 175$ GeV and to pass tight identification and isolation criteria, to ensure a high trigger efficiency of 98%.

5.2 Signal extraction

A binned likelihood fit to the data as presented in Ref. [14] is performed simultaneously in the five different control samples and in the signal region, for events selected in both the monojet and mono-V categories, to estimate the Z($\nu\nu$)+jets and W($\ell\nu$)+jets rate in each p_T^{miss} bin. In this likelihood, the expected numbers of Z($\nu\nu$)+jets events in each bin of p_T^{miss} are the free parameters of the fit. Transfer factors, derived from simulation, are used to link the yields of the Z($\ell\ell$)+jets, W($\ell\nu$)+jets and γ +jets processes in the control regions with the Z($\nu\nu$)+jets and W($\ell\nu$)+jets background estimates in the signal region. These transfer factors are defined as the ratio of expected yields of the target process in the signal region and the process being measured in the control sample.

To estimate the W($\ell\nu$)+jets background in the signal region, the transfer factors between the W($\mu\nu$)+jets and W($e\nu$)+jets event yields in the single-lepton control samples and the estimates of the W($\ell\nu$)+jets background in the signal region are constructed. These transfer factors take into account the impact of lepton acceptances and efficiencies, lepton veto efficiencies, and the difference in the trigger efficiencies in the case of the single-electron control sample.

The Z $\rightarrow \nu\nu$ background prediction in the signal region is connected to the yields of Z $\rightarrow \mu^+\mu^-$ and Z $\rightarrow e^+e^-$ events in the dilepton control samples. The associated transfer factors account for the differences in the branching ratio of Z bosons to charged leptons relative to neutrinos and the impact of lepton acceptance and selection efficiencies. In the case of dielec-

tron events, the transfer factor also takes into account the difference in the trigger efficiencies. The resulting constraint on the $Z(\nu\nu)+\text{jets}$ process from the dilepton control samples is limited by the statistical uncertainty in the dilepton control samples because of the large difference in branching fractions between Z boson decays to neutrinos and Z boson decays to muons and electrons.

The $\gamma+\text{jets}$ control sample is also used to predict the $Z(\nu\nu)+\text{jets}$ process in the signal region through a transfer factor, which accounts for the difference in the cross sections of the $\gamma+\text{jets}$ and $Z(\nu\nu)+\text{jets}$ processes, the effect of acceptance and efficiency of identifying photons along with the difference in the efficiencies of the photon and p_T^{miss} triggers. The addition of the $\gamma+\text{jets}$ control sample mitigates the impact of the limited statistical power of the dilepton constraint, because of the larger production cross section of $\gamma+\text{jets}$ process compared to that of $Z(\nu\nu)+\text{jets}$ process.

Finally, a transfer factor is also defined to connect the $Z(\nu\nu)+\text{jets}$ and $W(\ell\nu)+\text{jets}$ background yields in the signal region, to further benefit from the larger statistical power that the $W(\ell\nu)+\text{jets}$ background provides, making it possible to experimentally constrain $Z(\nu\nu)+\text{jets}$ production at high p_T^{miss} .

These transfer factors rely on an accurate prediction of the ratio of Z+jets, W+jets, and $\gamma+\text{jets}$ cross sections. Therefore, LO simulations for these processes are corrected using boson p_T -dependent NLO QCD K-factors derived using MADGRAPH5_aMC@NLO. They are also corrected using p_T -dependent higher-order EW corrections extracted from theoretical calculations [78–83]. The higher-order corrections are found to improve the data-to-simulation agreement for both the absolute prediction of the individual Z+jets, W+jets, and $\gamma+\text{jets}$ processes, and their respective ratios.

The remaining backgrounds that contribute to the total event yield in the signal region are much smaller than those from $Z(\nu\nu)+\text{jets}$ and $W(\ell\nu)+\text{jets}$ processes. These smaller backgrounds include QCD multijet events which are measured from data using a $\Delta\phi$ extrapolation method [14, 84], and top quark and diboson processes, which are obtained directly from simulation.

5.3 Systematic uncertainties

Systematic uncertainties in the transfer factors are modeled as constrained nuisance parameters and include both experimental and theoretical uncertainties in the $\gamma+\text{jets}$ to Z+jets and W+jets to Z+jets differential cross section ratios.

Theoretical uncertainties in V-jets and $\gamma+\text{jets}$ processes include effects from QCD and EW higher-order corrections along with PDF modeling uncertainty. To estimate the theoretical uncertainty in the V-jets and $\gamma+\text{jets}$ ratios due to QCD and EW higher-order effects as well as their correlations across the processes and p_T bins, the recommendations of Ref. [16] are employed, as detailed in the following explanation.

Three separate sources of uncertainty associated with QCD higher order corrections are used. One of the uncertainties considered comes from the variations around the central renormalization and factorization scale choice. It is evaluated by taking the differences in the NLO cross section as a function of boson p_T after changing the renormalization and factorization scales by a factor of two and a factor of one-half with respect to the default value. These constant scale variations mainly affect the overall normalization of the boson p_T distributions and therefore underestimate the shape uncertainties that play an important role in the extrapolation of low- p_T measurements to high- p_T . A second, conservative shape uncertainty derived from altered

boson p_T spectra is used to supplement the scale uncertainties and account for the p_T dependence of the uncertainties. The modeling of the correlations between the processes assumes a close similarity of QCD effects between all V-jets and γ +jets processes. However, the QCD effects in γ +jets production could differ compared to the case of Z+jets and W+jets productions. In order to account for this variation, a third uncertainty is computed based on the difference of the known QCD K-factors of the W+jets and γ +jets processes with respect to Z+jets production. All QCD uncertainties are correlated across the Z+jets, W+jets, γ +jets processes, and also correlated across the bins of the hadronic recoil p_T .

For the V-jets and γ +jets processes, nNLO EW corrections are applied, which correspond to full NLO EW corrections [78–80, 83] supplemented by two-loop Sudakov EW logarithms [81, 85–87]. We also considered three separate sources of uncertainty arising from the following: pure EW higher-order corrections failing to cover the effects of unknown Sudakov logarithms in the perturbative expansion beyond NNLO, missing NNLO effects that are not included in the nNLO EW calculations, and the difference between the next-to-leading logarithmic (NLL) Sudakov approximation at two-loop and simple exponentiation of the full NLO EW correction. The variations due to the effect of unknown Sudakov logs are correlated across the Z+jets, W+jets, and γ +jets processes and are also correlated across the bins of hadronic recoil p_T . On the other hand, the other two sources of EW uncertainties are treated as uncorrelated across the V-jet and γ +jets processes, and an independent nuisance parameter is used for each process.

A recommendation that includes a factorized approach to partially include mixed QCD-EW corrections is outlined in Ref. [16]. An additional uncertainty is introduced to account for the difference between the corrections done in the multiplicative and the additive approaches, to account for the non-factorized mixed EW-QCD effects.

The summary of the aforementioned theoretical uncertainties including their magnitude and correlation is outlined in Table 3.

Experimental uncertainties including the reconstruction efficiency (1% per muon or electron) and the selection efficiencies of leptons (1% per muon and 2% per electron), photons (2%), and hadronically decaying τ leptons (5%), are also incorporated. These reconstruction and selection efficiencies further translate into an uncertainty in the lepton veto efficiency of 3%. Uncertainties in the purity of photons in the γ +jets control sample (2%), and in the efficiency of the electron (2%), photon (2%), and p_T^{miss} (1–4%) triggers, are included and are fully correlated across all the bins of hadronic recoil p_T and p_T^{miss} . The uncertainty in the efficiency of the b jet veto is estimated to be 6% (2)% for the contribution of the top quark (diboson) background.

The uncertainty in the efficiency of the V tagging requirements is estimated to be 9% in the mono-V category. The uncertainty in the modeling of p_T^{miss} in simulation [50] is estimated to be 4% and is dominated by the uncertainty in the jet energy scale.

A systematic uncertainty of 10% is included for the top quark background associated with the modeling of the top quark p_T distribution in simulation [88]. In addition, systematic uncertainties of 10 and 20% are included in the normalizations of the top quark [89] and diboson backgrounds [90, 91], respectively, to account for the uncertainties in their cross sections in the relevant kinematic phase space. Lastly, the uncertainty in the QCD multijet background estimate is found to be between 50–150% due to the variations of the jet response and the statistical uncertainty of the extrapolation factors.

Table 3: Theoretical uncertainties considered in the V-jets and γ +jets processes, and their ratios. The correlation between each process and between the p_T bins are described.

Uncertainty source	Process (magnitude)	Correlation
Fact. & renorm. scales (QCD)	$Z \rightarrow \nu\nu/W \rightarrow \ell\nu$ (0.1 – 0.5%) $Z \rightarrow \nu\nu/\gamma$ +jets (0.2 – 0.5%)	Correlated between processes; and in p_T
p_T shape dependence (QCD)	$Z \rightarrow \nu\nu/W \rightarrow \ell\nu$ (0.4 – 0.1%) $Z \rightarrow \nu\nu/\gamma$ +jets (0.1 – 0.2%)	Correlated between processes; and in p_T
Process dependence (QCD)	$Z \rightarrow \nu\nu/W \rightarrow \ell\nu$ (0.4 – 1.5%) $Z \rightarrow \nu\nu/\gamma$ +jets (1.5 – 3.0%)	Correlated between processes; and in p_T
Effects of unknown Sudakov logs (EW)	$Z \rightarrow \nu\nu/W \rightarrow \ell\nu$ (0 – 0.5%) $Z \rightarrow \nu\nu/\gamma$ +jets (0.1 – 1.5%)	Correlated between processes; and in p_T
Missing NNLO effects (EW)	$Z \rightarrow \nu\nu$ (0.2 – 3.0%) $W \rightarrow \ell\nu$ (0.4 – 4.5%) γ +jets (0.1 – 1.0%)	Uncorrelated between processes; correlated in p_T
Effects of NLL Sudakov approx. (EW)	$Z \rightarrow \nu\nu$ (0.2 – 4.0%) $W \rightarrow \ell\nu$ (0 – 1.0%) γ +jets (0.1 – 3.0%)	Uncorrelated between processes; correlated in p_T
Unfactorized mixed QCD-EW corrections	$Z \rightarrow \nu\nu/W \rightarrow \ell\nu$ (0.15 – 0.3%) $Z \rightarrow \nu\nu/\gamma$ +jets (<0.1%)	Correlated between processes; and in p_T
PDF	$Z \rightarrow \nu\nu/W \rightarrow \ell\nu$ (0 – 0.3%) $Z \rightarrow \nu\nu/\gamma$ +jets (0 – 0.6%)	Correlated between processes; and in p_T

5.4 Control sample validation

An important cross-check of the application of p_T -dependent NLO QCD and EW corrections is represented by the agreement between data and simulation in the ratio of Z+jets events to both γ +jets events and W+jets events in the control samples, as a function of hadronic recoil p_T .

Figure 4 shows the ratio between Z($\ell\ell$)+jets and γ +jets (left), Z($\ell\ell$)+jets and W($\ell\nu$)+jets (middle), and the one between W($\ell\nu$)+jets/ γ +jets processes (right) as a function of the recoil for events selected in the monojet category. While we do not explicitly use a W($\ell\nu$)+jets/ γ +jets constraint in the analysis, the two cross sections are connected through the Z+jets/ γ +jets and Z+jets/W+jets constraints that are explained in Section 5.2. Therefore, it is instructive to examine the data-MC comparison of the W($\ell\nu$)+jets/ γ +jets ratio. Good agreement is observed between data and simulation after the application of the NLO corrections as shown in Fig. 4. The ratio between Z($\mu\mu$)+jets and γ +jets, Z($\mu\mu$)+jets and W($\mu\nu$)+jets and the one between W($\mu\nu$)+jets/ γ +jets processes as a function of the boson p_T is also studied and the results can be seen in Fig. 19 in Section A.

Figures 5–7 show the results of the combined fit in all control samples and the signal region. Data in the control samples are compared to the pre-fit predictions from simulation and the post-fit estimates obtained after performing the fit. The control samples with larger yields dominate the fit results. A normalization difference of 7% is observed in the pre-fit distributions for the mono-V category in the single-lepton and dilepton control regions. The sources of the differences are identified to be the modeling of the pruned mass variable and the large theoretical uncertainties in the diboson and top quark backgrounds, which are the leading backgrounds in these regions. The normalization difference is found to be fully mitigated by the fitting procedure.

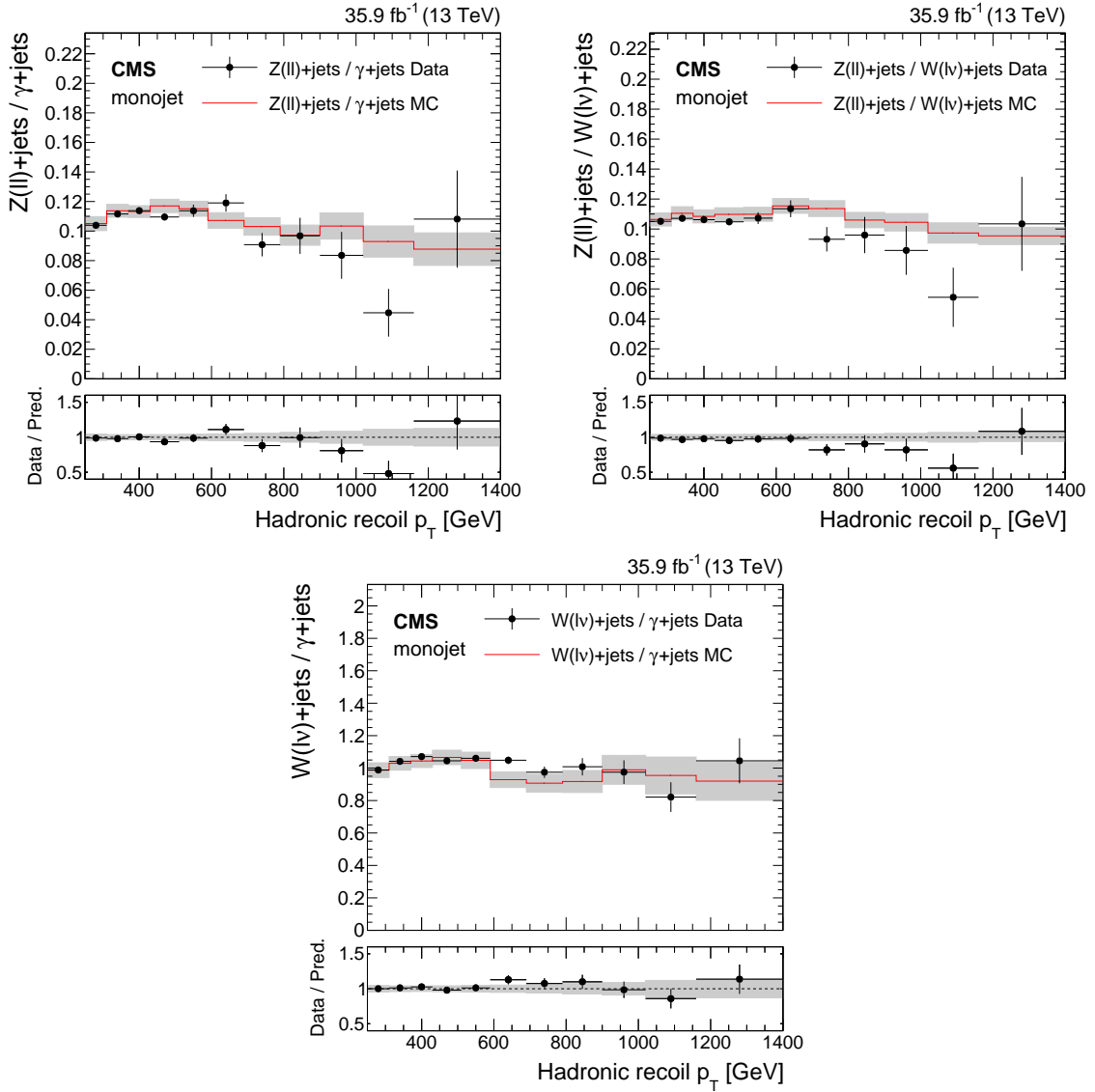


Figure 4: Comparison between data and MC simulation for the $Z(\ell\ell)/\gamma+jets$, $Z(\ell\ell)/W(\ell\nu)$, and $W(\ell\nu)/\gamma+jets$ ratios as a function of the hadronic recoil in the monojet category. In the lower panels, ratios of data with the pre-fit background prediction are shown. The gray bands include both the pre-fit systematic uncertainties and the statistical uncertainty in the simulation.

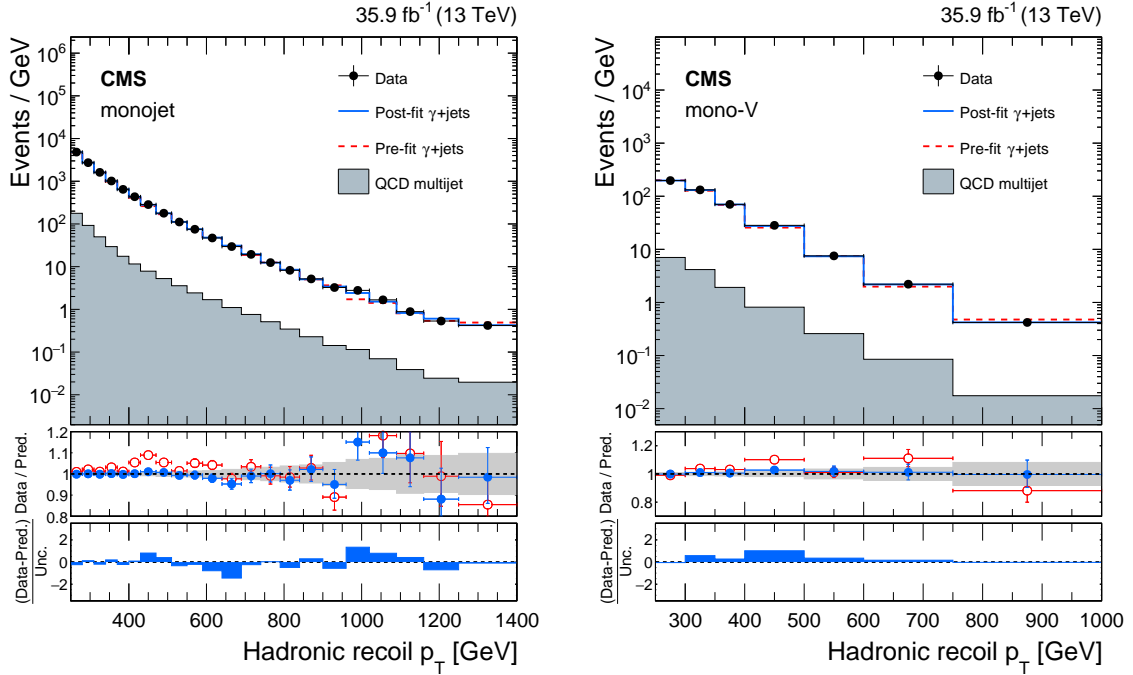


Figure 5: Comparison between data and MC simulation in the γ +jets control sample before and after performing the simultaneous fit across all the control samples and the signal region assuming the absence of any signal. The left plot shows the monojet category and the right plot shows the mono-V category. The hadronic recoil p_T in γ +jets events is used as a proxy for p_T^{miss} in the signal region. The last bin includes all events with hadronic recoil p_T larger than 1250 (750) GeV in the monojet (mono-V) category. In the lower panels, ratios of data with the pre-fit background prediction (red open points) and post-fit background prediction (blue full points) are shown for both the monojet and mono-V categories. The gray band in the lower panel indicates the post-fit uncertainty after combining all the systematic uncertainties. Finally, the distribution of the pulls, defined as the difference between data and the post-fit background prediction relative to the quadrature sum of the post-fit uncertainty in the prediction and statistical uncertainty in data, is shown in the lowest panel.

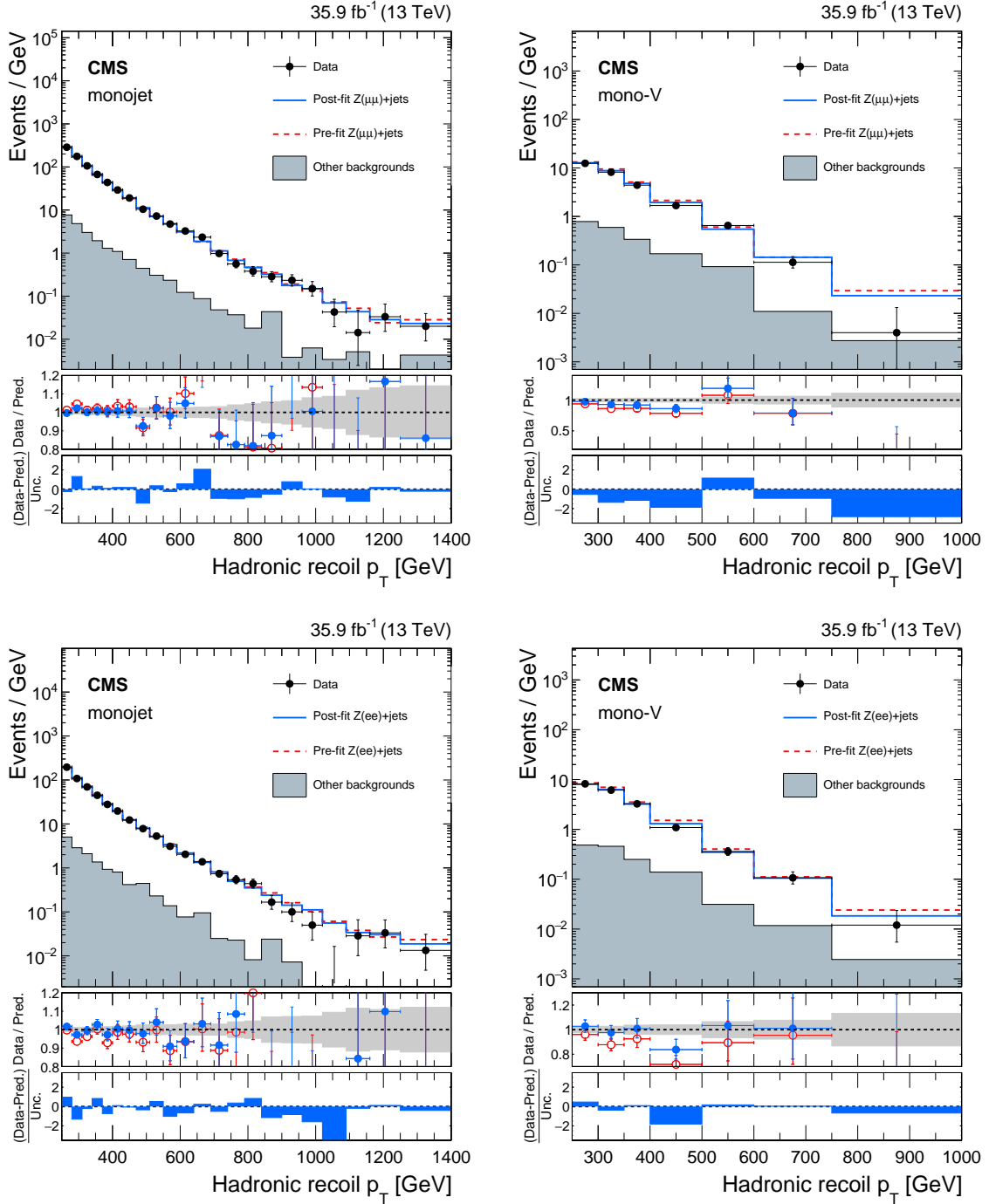


Figure 6: Comparison between data and MC simulation in the dimuon (upper row) and dielectron (lower row) control samples before and after performing the simultaneous fit across all the control samples and the signal region assuming the absence of any signal. Plots correspond to the monojet (left) and mono-V (right) categories, respectively, in the dilepton control sample. The hadronic recoil p_T in dilepton events is used as a proxy for p_T^{miss} in the signal region. The other backgrounds include top quark, diboson, and W +jets processes. The description of the lower panels is the same as in Fig. 5.

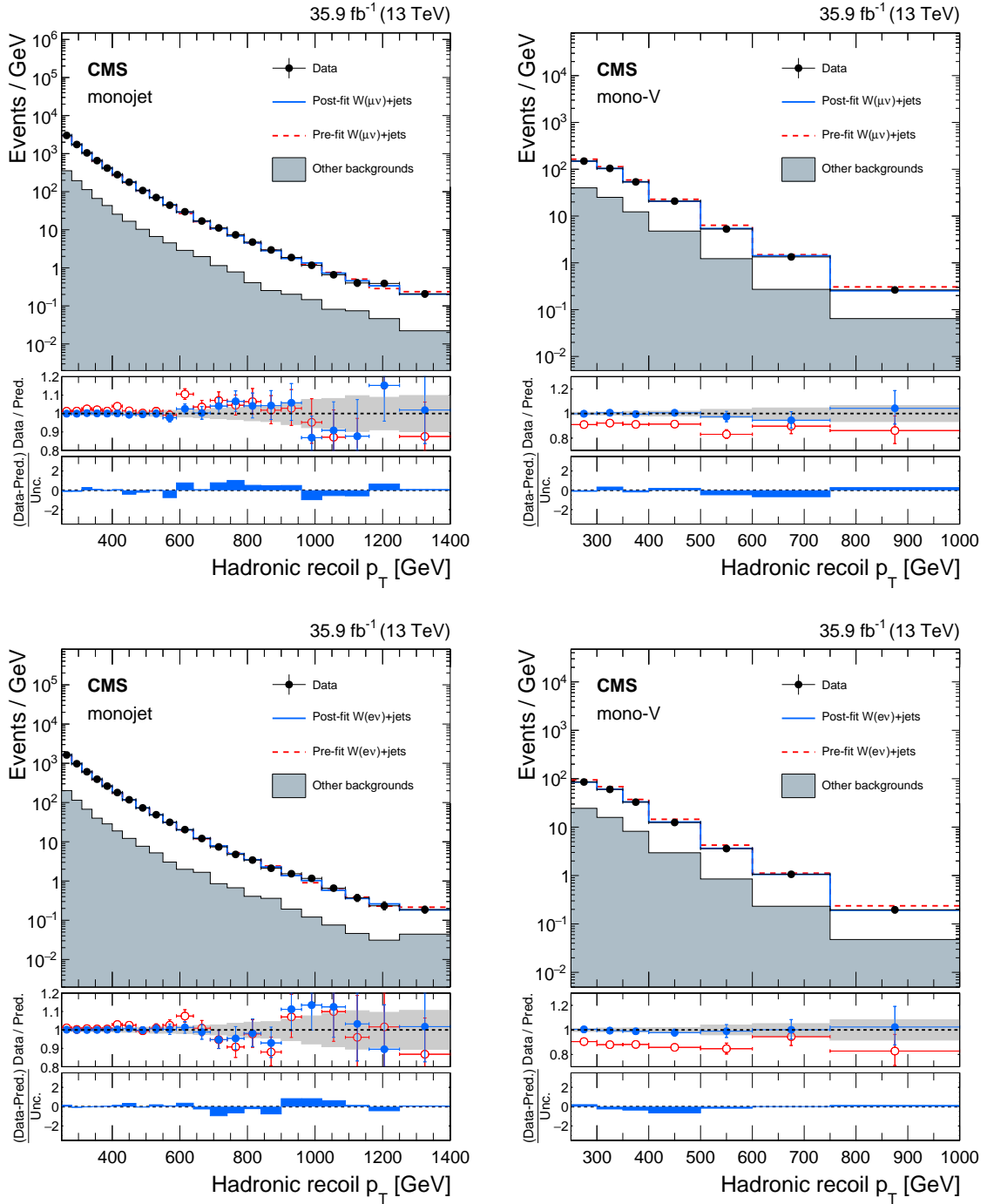


Figure 7: Comparison between data and MC simulation in the single-muon (upper row) and single-electron (lower row) control samples before and after performing the simultaneous fit across all the control samples and the signal region assuming the absence of any signal. Plots correspond to the monojet (left) and mono-V (right) categories, respectively, in the single-lepton control samples. The hadronic recoil p_T in single-lepton events is used as a proxy for p_T^{miss} in the signal region. The other backgrounds include top quark, diboson, and QCD multijet processes. The description of the lower panels is the same as in Fig. 5.

6 Results and interpretation

The search is performed by extracting the signal through a combined fit of the signal and control regions. Figure 8 shows the comparison between data and the post-fit background predictions in the signal region in the monojet and mono-V categories, where the background prediction is obtained from a combined fit performed in all control regions, excluding the signal region. Expected signal distributions for the 125 GeV Higgs boson decaying exclusively to invisible particles, and a 2 TeV axial-vector mediator decaying to 1 GeV DM particles, are overlaid. Data are found to be in agreement with the SM prediction.

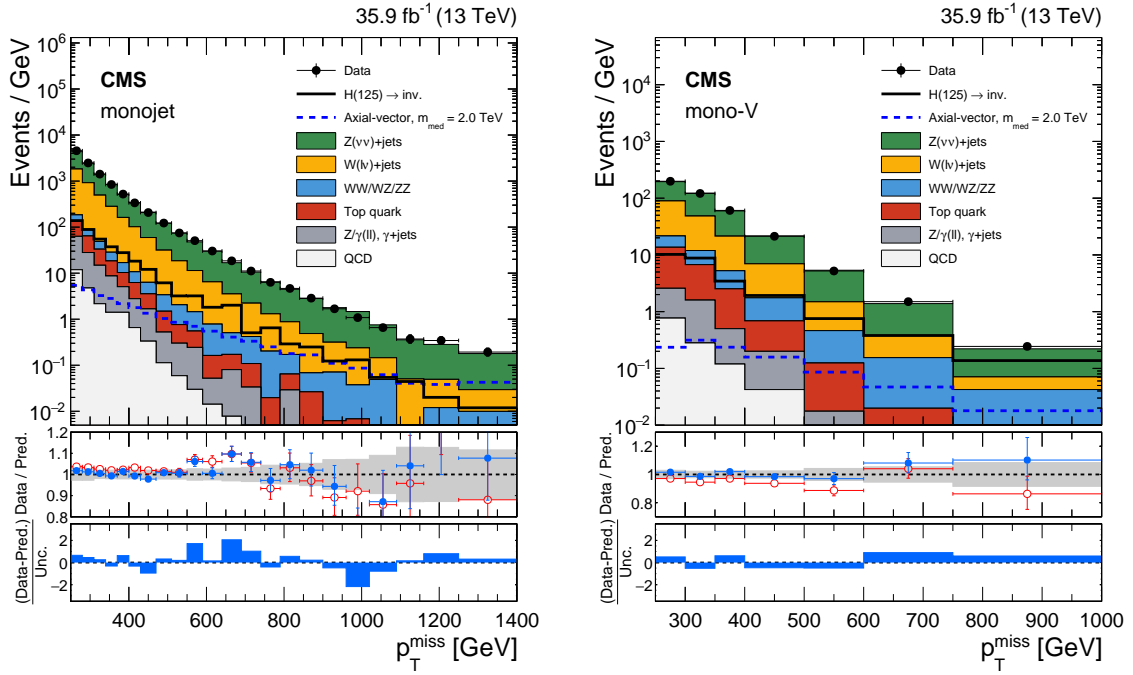


Figure 8: Observed p_T^{miss} distribution in the monojet (left) and mono-V (right) signal regions compared with the post-fit background expectations for various SM processes. The last bin includes all events with $p_T^{\text{miss}} > 1250$ (750) GeV for the monojet (mono-V) category. The expected background distributions are evaluated after performing a combined fit to the data in all the control samples, not including the signal region. Expected signal distributions for the 125 GeV Higgs boson decaying exclusively to invisible particles, and a 2 TeV axial-vector mediator decaying to 1 GeV DM particles, are overlaid. The description of the lower panels is the same as in Fig. 5.

The expected yields in each bin of p_T^{miss} for all SM backgrounds, after the fit to the data in the control regions, are given in Tables 4 and 5 for the monojet and mono-V signal regions, respectively. The correlations between the predicted background yields across all the p_T^{miss} bins in the two signal regions are shown in Figs. 20 and 21 in Section A. The expected yields together with the correlations can be used with the simplified likelihood approach detailed in Ref. [92] to reinterpret the results for models not studied in this paper.

Figure 9 shows a comparison between data and the post-fit background predictions in the signal region in the monojet and mono-V categories, where the fit is performed under the background-only hypothesis including signal region events in the likelihood. The limits on the production cross section of the various models described below is set after comparing this

Table 4: Expected event yields in each p_T^{miss} bin for various background processes in the monojet signal region. The background yields and the corresponding uncertainties are obtained after performing a combined fit to data in all the control samples, excluding data in the signal region. The other backgrounds include QCD multijet and γ +jets processes. The expected signal contribution for a 2 TeV axial-vector mediator decaying to 1 GeV DM particles and the observed event yields in the monojet signal region are also reported.

p_T^{miss} (GeV)	Signal	Z($\nu\nu$)+jets	W($\ell\nu$)+jets	Top quark	Diboson	Other	Total bkg.	Data
250-280	162 ± 3	79700 ± 2300	49200 ± 1400	2360 ± 200	1380 ± 220	1890 ± 240	134500 ± 3700	136865
280-310	130 ± 3	45800 ± 1300	24950 ± 730	1184 ± 99	770 ± 120	840 ± 110	73400 ± 2000	74340
310-340	97.8 ± 2.4	27480 ± 560	13380 ± 260	551 ± 53	469 ± 77	445 ± 63	42320 ± 810	42540
340-370	84.8 ± 2.1	17020 ± 350	7610 ± 150	292 ± 28	301 ± 51	260 ± 39	25490 ± 490	25316
370-400	65.2 ± 1.9	10560 ± 220	4361 ± 91	157 ± 17	198 ± 33	152 ± 26	15430 ± 310	15653
400-430	53.5 ± 1.8	7110 ± 130	2730 ± 47	104 ± 12	133 ± 23	84 ± 15	10160 ± 170	10092
430-470	53.9 ± 1.8	6110 ± 100	2123 ± 37	75.2 ± 7.9	110 ± 19	67 ± 11	8480 ± 140	8298
470-510	41.4 ± 1.5	3601 ± 75	1128 ± 22	38.6 ± 5.3	75 ± 12	21.0 ± 3.9	4865 ± 95	4906
510-550	34.3 ± 1.4	2229 ± 39	658 ± 12	18.5 ± 3.3	51.7 ± 9.5	12 ± 2.4	2970 ± 49	2987
550-590	28.1 ± 1.2	1458 ± 27	398 ± 8	12.3 ± 2.6	35.9 ± 7.1	9.7 ± 1.9	1915 ± 33	2032
590-640	27.5 ± 1.2	1182 ± 26	284 ± 7	5.5 ± 1.4	30.9 ± 5.7	2.6 ± 0.7	1506 ± 32	1514
640-690	20.4 ± 1.1	667 ± 15	151 ± 4	4.6 ± 1.7	16.7 ± 3.9	4.0 ± 0.8	844 ± 18	926
690-740	16.6 ± 0.9	415 ± 12	90.4 ± 3.0	3.8 ± 1.5	15.6 ± 3.6	1.7 ± 0.4	526 ± 14	557
740-790	12.5 ± 0.8	259 ± 9.6	55.2 ± 2.3	0.8 ± 0.5	9.14 ± 2.3	0.2 ± 0.1	325 ± 12	316
790-840	8.94 ± 0.72	178 ± 7.1	35.3 ± 1.7	1.7 ± 0.8	5.35 ± 1.7	1.4 ± 0.3	223 ± 9	233
840-900	10.1 ± 0.7	139 ± 6.2	25.2 ± 1.3	1.5 ± 1.2	2.52 ± 1.05	0.04 ± 0.03	169 ± 8	172
900-960	6.62 ± 0.61	88.1 ± 4.9	14.7 ± 0.9	0.3 ± 0.3	3.88 ± 1.42	0.03 ± 0.02	107 ± 6	101
960-1020	5.19 ± 0.54	73.8 ± 4.7	12.0 ± 0.8	0.4 ± 0.3	1.83 ± 0.92	0.02 ± 0.01	88.1 ± 5.3	65
1020-1090	4.35 ± 0.52	42.6 ± 3.1	6.7 ± 0.6	0.0 ± 0.0	3.42 ± 1.33	0.01 ± 0.01	52.8 ± 3.9	46
1090-1160	2.84 ± 0.43	21.5 ± 2.1	3.5 ± 0.4	0.0 ± 0.0	0.00 ± 0.00	0.01 ± 0.00	25.0 ± 2.5	26
1160-1250	3.44 ± 0.38	21.0 ± 2.2	3.3 ± 0.4	0.0 ± 0.0	1.07 ± 0.69	0.01 ± 0.00	25.5 ± 2.6	31
>1250	6.39 ± 0.58	22.5 ± 2.4	2.9 ± 0.3	0.0 ± 0.0	1.49 ± 0.91	0.01 ± 0.00	26.9 ± 2.8	29

fit with an alternative one assuming the presence of signal.

6.1 Dark matter interpretation

The results are interpreted in terms of simplified s -channel DM models assuming a vector, axial-vector, scalar, or pseudoscalar mediator decaying into a pair of fermionic DM particles. The coupling of the mediators to the DM is assumed to be unity for all four types of mediators. The spin-0 particles are assumed to couple to the quarks with a coupling strength (g_q) of 1. In the case of the spin-1 mediators, g_q is taken to be 0.25. The choice of all the signal model parameters follows the recommendations from Ref. [93]. Uncertainties of 20 and 30% are assigned to the inclusive signal cross section in the case of the spin-1 and spin-0 mediators, respectively. These estimates include the renormalization and factorization scale uncertainties, as well as the PDF uncertainty.

Upper limits are computed at 95% CL on the ratio of the measured signal cross section to the predicted one, denoted by $\mu = \sigma/\sigma_{\text{th}}$, with the CL_s method [94, 95], using the asymptotic approximation [96]. Limits are obtained as a function of the mediator mass (m_{med}) and the DM mass (m_{DM}). Figure 10 shows the exclusion contours in the $m_{\text{med}}-m_{\text{DM}}$ plane for the vector and axial-vector mediators. Mediator masses up to 1.8 TeV, and DM masses up to 700 and 500 GeV are excluded for the vector and axial-vector models, respectively. Figure 11 shows the limits for the scalar mediators as a function of the mediator mass, for a fixed DM mass of 1 GeV and the exclusion contours in the $m_{\text{med}}-m_{\text{DM}}$ plane for pseudoscalar mediators, respectively. Pseudoscalar mediator (dark matter) masses up to 400 (150) GeV are excluded at 95% CL. A

Table 5: Expected event yields in each p_T^{miss} bin for various background processes in the mono-V signal region. The background yields and the corresponding uncertainties are obtained after performing a combined fit to data in all the control samples, but excluding data in the signal region. The other backgrounds include QCD multijet and γ +jets processes. The expected signal contribution for a 2 TeV axial-vector mediator decaying to 1 GeV DM particles and the observed event yields in the mono-V signal region are also reported.

p_T^{miss} (GeV)	Signal	Z($\nu\nu$)+jets	W($\ell\nu$)+jets	Top quark	Diboson	Other	Total bkg.	Data
250-300	11.7 ± 0.6	5300 ± 170	3390 ± 120	553 ± 54	396 ± 69	128 ± 25	9770 ± 290	9929
300-350	15.7 ± 0.7	3720 ± 98	1823 ± 53	257 ± 27	261 ± 46	79.8 ± 13	6140 ± 140	6057
350-400	11.8 ± 0.6	1911 ± 59	808 ± 28	101 ± 12	134 ± 25	25.0 ± 4.8	2982 ± 79	3041
400-500	15.8 ± 0.7	1468 ± 45	521 ± 15	48.8 ± 5.7	107 ± 20	20.0 ± 3.6	2165 ± 55	2131
500-600	8.59 ± 0.56	388 ± 18	103.0 ± 5.1	10.7 ± 1.9	33.8 ± 7.0	1.76 ± 0.53	537 ± 23	521
600-750	7.04 ± 0.47	151.0 ± 9.9	33.4 ± 2.3	1.9 ± 1.1	20.2 ± 4.5	1.05 ± 0.25	208 ± 11	225
>750	4.48 ± 0.40	37.7 ± 3.7	7.09 ± 0.69	0.28 ± 0.25	10.2 ± 2.3	0.06 ± 0.03	55.3 ± 4.6	61

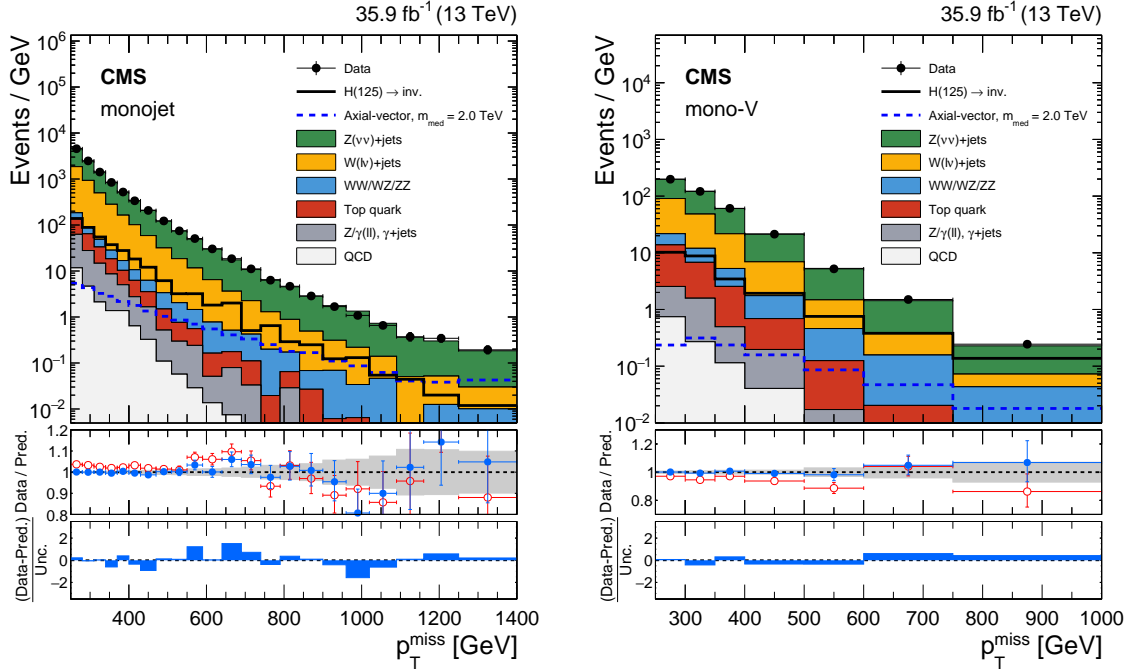


Figure 9: Observed p_T^{miss} distribution in the monojet (left) and mono-V (right) signal regions compared with the post-fit background expectations for various SM processes. The last bin includes all events with $p_T^{\text{miss}} > 1250$ (750) GeV for the monojet (mono-V) category. The expected background distributions are evaluated after performing a combined fit to the data in all the control samples, as well as in the signal region. The fit is performed assuming the absence of any signal. Expected signal distributions for the 125 GeV Higgs boson decaying exclusively to invisible particles, and a 2 TeV axial-vector mediator decaying to 1 GeV DM particles, are overlaid. The description of the lower panels is the same as in Fig. 5.

direct comparison of the results for simplified DM models of this paper, to the one presented in Ref. [14] can be seen in Fig. 22 and Fig. 23 in Section A.

The results for vector, axial-vector, and pseudoscalar mediators are compared to constraints

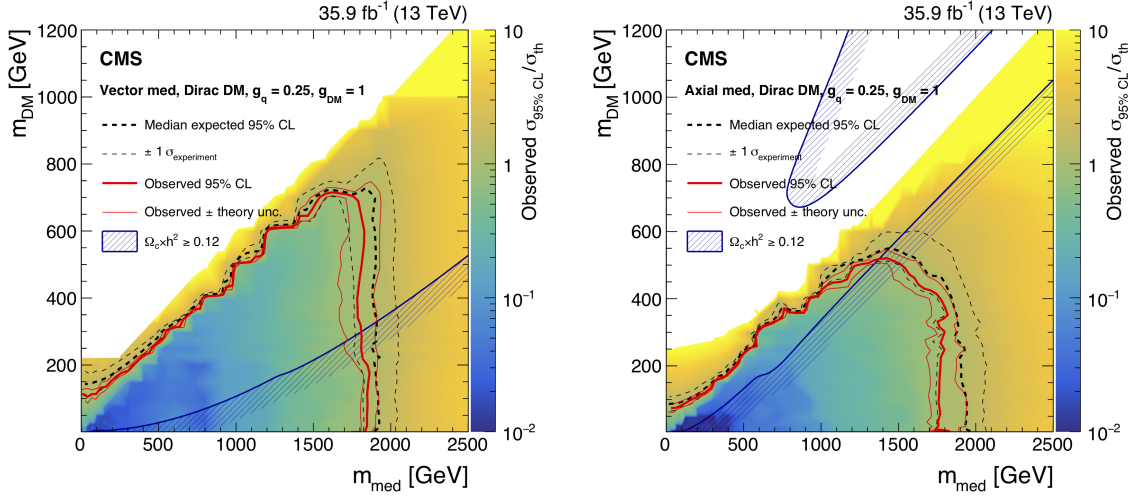


Figure 10: Exclusion limits at 95% CL on $\mu = \sigma/\sigma_{\text{th}}$ in the $m_{\text{med}}-m_{\text{DM}}$ plane assuming vector (left) and axial-vector (right) mediators. The solid (dotted) red (black) line shows the contour for the observed (expected) exclusion. The solid contours around the observed limit and the dashed contours around the expected limit represent one standard deviation due to theoretical uncertainties in the signal cross section and the combination of the statistical and experimental systematic uncertainties, respectively. Constraints from the Planck satellite experiment [97] are shown as dark blue contours; in the shaded area DM is overabundant.

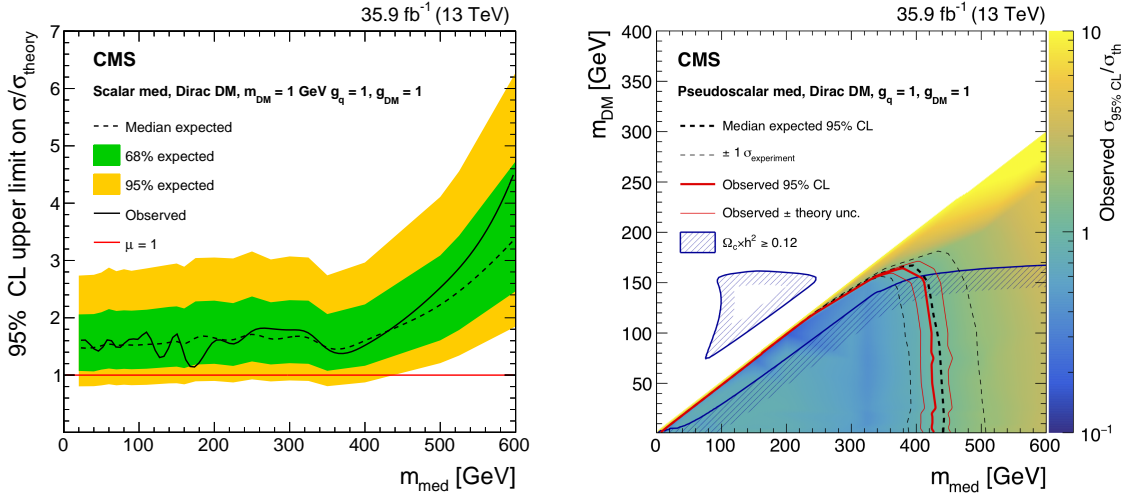


Figure 11: Expected (dotted black line) and observed (solid black line) 95% CL upper limits on the signal strength $\mu = \sigma/\sigma_{\text{th}}$ as a function of the mediator mass for the scalar mediators (left) for $m_{\text{DM}} = 1 \text{ GeV}$. The horizontal red line denotes $\mu = 1$. Exclusion limits at 95% CL on $\mu = \sigma/\sigma_{\text{th}}$ in the $m_{\text{med}}-m_{\text{DM}}$ plane assuming pseudoscalar mediators (right). The solid (dashed) red (black) line shows the contours for the observed (expected) exclusion. Constraints from the Planck satellite experiment [97] are shown with the dark blue contours; in the shaded area DM is overabundant.

from the observed cosmological relic density of DM as determined from measurements of the cosmic microwave background by the Planck satellite experiment [97]. The expected DM abundance is estimated, separately for each model, using the thermal freeze-out mechanism

implemented in the MADDM [98] framework and compared to the observed cold DM density $\Omega_c h^2 = 0.12$ [99], where Ω_c is the DM relic abundance and h is the Hubble constant.

In addition to scanning the $m_{\text{med}}-m_{\text{DM}}$ plane, for a fixed g_q value, the analysis interprets the results in the $m_{\text{med}}-g_q$ plane for a fixed ratio of $m_{\text{med}}/m_{\text{DM}} = 3$. The ratio is chosen to ensure a valid relic abundance solution for every allowed g_q value scanned for a spin-1 simplified model. Quark couplings down to 0.05 for mediator masses at 50 GeV are excluded for the spin-1 simplified models as shown in Fig. 12.

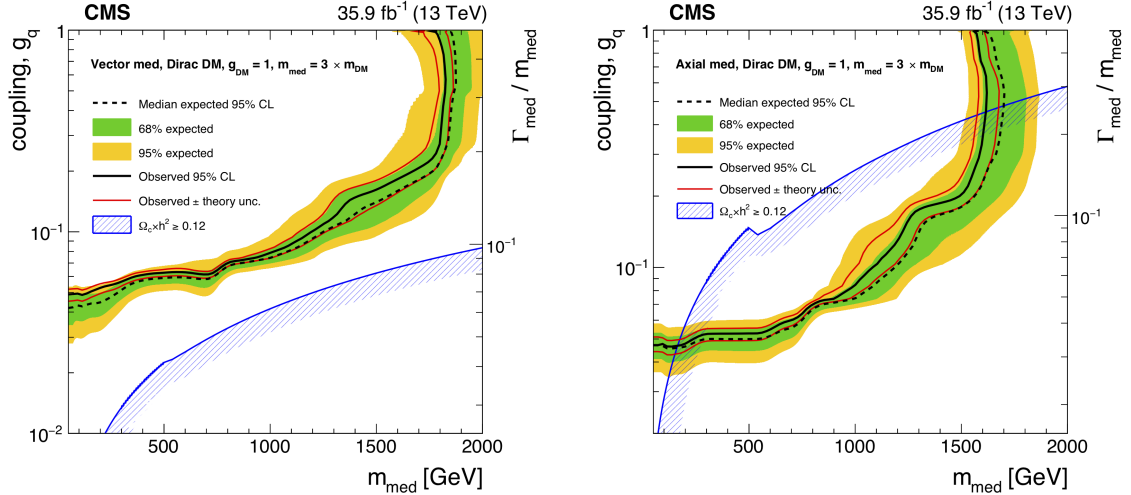


Figure 12: Exclusion limits at 95% CL on $\mu = \sigma/\sigma_{\text{th}}$ in the $m_{\text{med}}-g_q$ plane assuming vector (left) and axial-vector (right) mediators. The widths shown on the axis correspond to mediator masses above 400 GeV, where the top quark decay channel is fully open. For the mediator masses below the top quark decay channel threshold the width is 9% less. The solid (dotted) black line shows the contour for the observed (expected) exclusion. The solid red contours around the observed limit represent one standard deviation due to theoretical uncertainties in the signal cross section. Constraints from the Planck satellite experiment [97] are shown as dark blue contours; in the shaded area DM is overabundant.

The exclusion contours obtained from the simplified DM models are translated to 90%CL upper limits on the spin-independent/spin-dependent ($\sigma_{\text{SI/SD}}$) DM-nucleon scattering cross sections using the approach outlined in Refs. [19, 36, 100]. The results for the vector and axial-vector mediators are compared with the results of direct searches in Fig. 13. This search provides the most stringent constraints for vector mediators, for DM particle masses below 5 GeV. For axial-vector mediators, the sensitivity achieved in this search provides stronger constraints up to a DM particle mass of 550 GeV than those obtained from direct searches. For pseudoscalar mediators, the 90%CL upper limits as shown in Fig. 14 are translated to velocity-averaged DM annihilation cross section ($\langle\sigma v\rangle$) and are compared to the indirect detection results from the Fermi-LAT Collaboration [101]. The collider results provide stronger constraints for DM masses less than 150 GeV.

6.1.1 Fermion portal dark matter interpretation

The total production cross section in the fermion portal DM model has an exponential (linear) dependence on the mass of the new scalar mediator m_{ϕ_u} (mass of the DM candidate m_χ). The middle diagram shown in Fig. 1 represents the main production mechanism for small m_{ϕ_u} values, whereas the right diagram contributes to the total cross section for $m_{\phi_u} > 1$ TeV. The

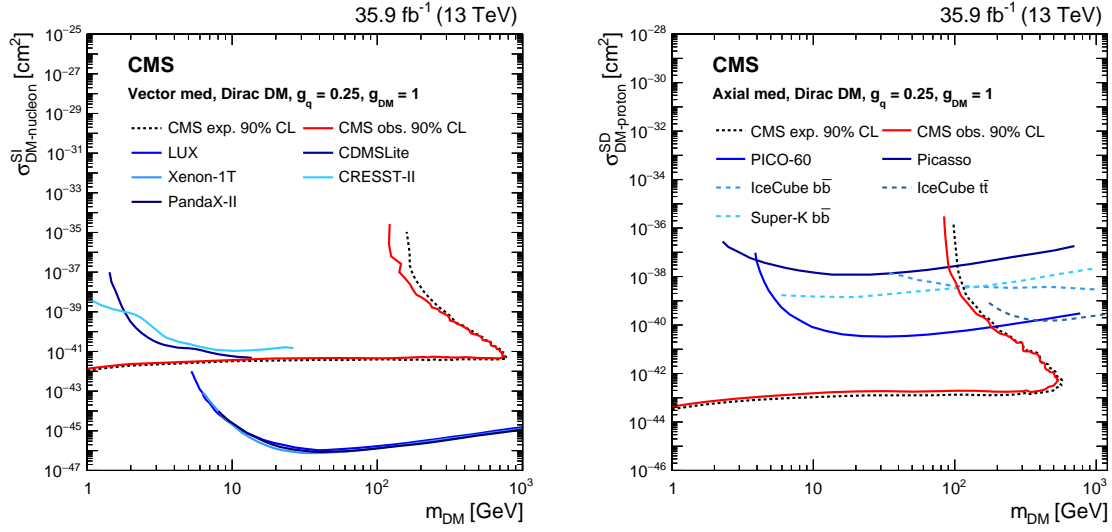


Figure 13: Exclusion limits at 90%CL in the m_{DM} vs. $\sigma_{\text{SI/SD}}$ plane for vector (left) and axial-vector (right) mediator models. The solid red (dotted black) line shows the contour for the observed (expected) exclusion in this search. Limits from CDMSLite [102], LUX [103], XENON-1T [104], PANDAX-II [105], and CRESST-II [106] are shown for the vector mediator. Limits from Picasso [107], PICO-60 [108], IceCube [109], and Super-Kamiokande [110] are shown for the axial-vector mediator.

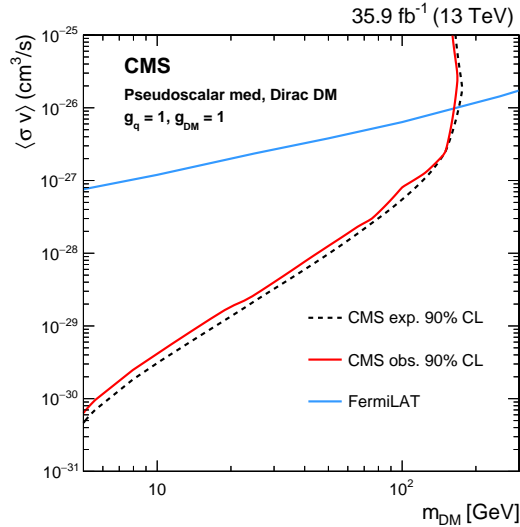


Figure 14: For the pseudoscalar mediator, limits are compared to the the velocity averaged DM annihilation cross section upper limits from Fermi-LAT [101]. There are no comparable limits from direct detection experiments, as the scattering cross section between DM particles and SM quarks is suppressed at nonrelativistic velocities for a pseudoscalar mediator [111, 112].

region where $m_{\phi_u} < m_\chi$ is not considered in the search, because of the reduced production cross section of the model. The upper limits on the signal strength are set as a function of m_{ϕ_u} and m_χ . Figure 15 shows the exclusion contours in the m_{ϕ_u} - m_χ plane, for which the coupling strength λ_u of the interaction between the scalar mediator and up-type quarks is fixed at unity. The results are also compared to constraints from the observed cosmological relic density of DM, obtained by the Planck satellite experiment, for the allowed values of m_{ϕ_u} and m_χ [20]. In this search, mediator (dark matter) masses up to 1.4 (0.6) TeV are excluded.

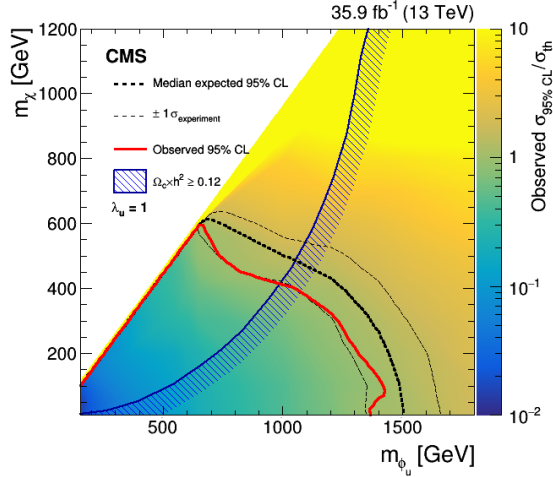


Figure 15: The 95% CL expected (black dashed line) and observed (red solid line) upper limits on $\mu = \sigma/\sigma_{\text{th}}$ in the context of the fermion portal DM model, for Dirac DM particles with coupling strengths to the up quark corresponding to $\lambda_u = 1$ in the m_{ϕ_u} - m_χ plane. Constraints from the Planck satellite experiment [97] are shown as dark blue contours; in the shaded area DM is overabundant.

6.1.2 Nonthermal dark matter interpretation

This search is also interpreted in the context of the nonthermal DM model where the DM candidate is not parity protected and therefore could be singly produced. Such production leads to signatures with an energetic jet and large p_T^{miss} whose distribution is characterized by a Jacobian-like shape, which exhibits a peak at half of the mediator mass. Therefore, multiple mediator mass points have been studied. The search is restricted to a coupling range of 0.01–1.5 for λ_1 and 0.01–2.0 for λ_2 to ensure the mediator width is less than about 30% of its mass. Within these bounds, no significant excesses were found and limits are reported as a function of coupling strength parameters λ_1 and λ_2 for two reference mediator masses m_{χ_1} of 1 and 2 TeV. Figure 16 shows the exclusion contours in the λ_1 - λ_2 plane.

6.2 Invisible decays of the Higgs boson interpretation

The results of this search are further interpreted in terms of an upper limit on the production cross section and branching fraction, $\mathcal{B}(H \rightarrow \text{inv.})$, where the Higgs boson is produced through gluon fusion (ggH) along with a jet; or in association with a vector boson (ZH, WH); or through vector boson fusion (VBF). The predictions for the Higgs boson production cross section and the corresponding theoretical uncertainties are taken from the recommendations of the LHC Higgs cross section working group [113]. The observed (expected) 95% CL upper limit on the invisible branching fraction of the Higgs boson, $\sigma \times \mathcal{B}(H \rightarrow \text{inv.})/\sigma_{\text{SM}}$, is found to be 53% (40%). The limits are summarized in Fig. 17, while Table 6 shows the individual limits for the monojet and mono-V categories.

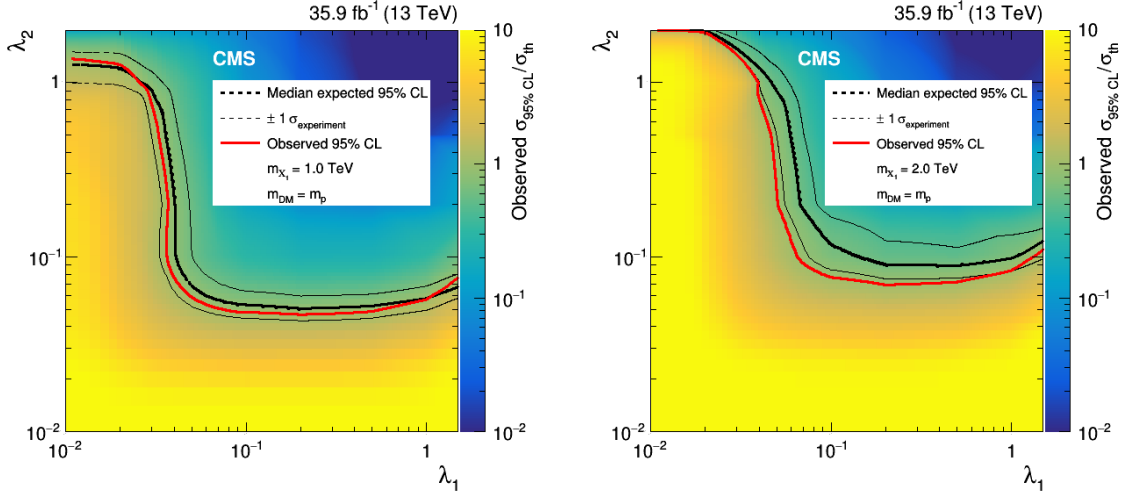


Figure 16: Expected (black line) and observed (red line) 95%CL upper limits on the signal strength $\mu = \sigma/\sigma_{\text{th}}$, in the context of a nonthermal dark matter model. Results are reported in the λ_1 - λ_2 plane, which represents the coupling strength of the interaction of the new scalar mediator with down-type quarks and DM with up-type quarks, respectively. Limits are shown for m_{χ_1} of 1 TeV (left) and 2 TeV (right).

Table 6: Expected and observed 95%CL upper limits on the invisible branching fraction of the Higgs boson. Limits are tabulated for the monojet and mono-V categories separately, and for their combination. The one standard deviation uncertainty range in the expected limits is listed. The expected composition of the production modes of a Higgs boson with a mass of 125 GeV is summarized, assuming SM production cross sections.

Category	Observed (expected)	68% expected	Expected signal composition
Monojet	0.74 (0.57)	0.40–0.86	72.8% ggH, 21.5% VBF, 3.3% WH, 1.9% ZH, 0.6% ggZH
mono-V	0.49 (0.45)	0.32–0.64	38.7% ggH, 7.0% VBF, 32.9% WH, 14.6% ZH, 6.7% ggZH
Combined	0.53 (0.40)	0.29–0.58	—

6.3 The ADD model interpretation

The 95%CL lower limits on the fundamental Planck scale M_D of the ADD model are presented as a function of the number of extra spatial dimensions n . The efficiency of the full event selection in the monojet (mono-V) category for this model ranges between 15 (1)% and 20 (1.5)% depending on the values of the parameters M_D and n . An upper limit on the signal strength $\mu = \sigma/\sigma_{\text{th}}$ is presented for the ADD graviton production for $n = 2$ EDs, as a function of M_D in Fig. 18. In addition, Fig. 18 shows the observed exclusion on M_D which varies from 9.9 TeV for $n = 2$ to 5.3 TeV for $n = 6$. The results of this search are also compared to earlier ones obtained by the CMS Collaboration with Run 1 data corresponding to an integrated luminosity of 19.7 fb^{-1} at a centre-of-mass energy of 8 TeV [10]. The upper limits on the signal production cross section and M_D exclusions are also provided in Table 7 as a function of the number of extra dimensions. Compared to previous CMS publications in this channel, the lower limits on M_D show a factor of 2 improvement.

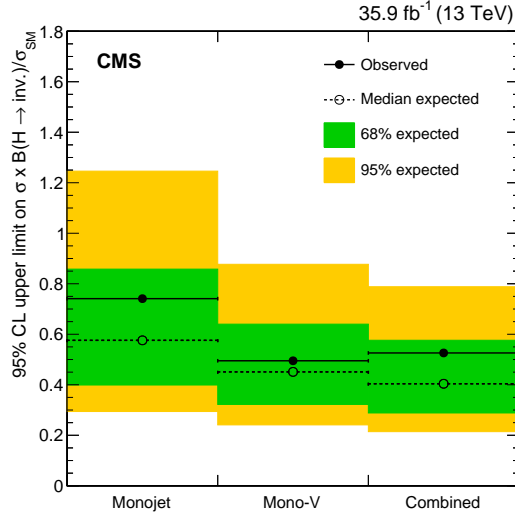


Figure 17: Expected (dotted line) and observed (solid line) 95% CL upper limits on the invisible branching fraction of the 125 GeV SM-like Higgs boson. Limits are shown for the monojet and mono-V categories separately, and also for their combination.

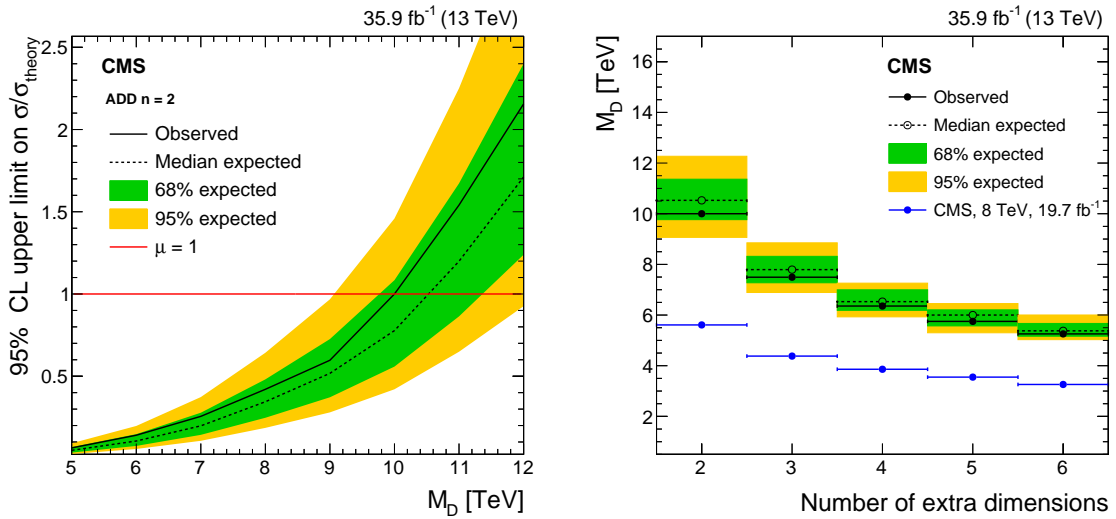


Figure 18: The 95% CL expected (dotted) and observed (solid) upper limits on the signal strength $\mu = \sigma/\sigma_{\text{th}}$ for ADD graviton production (left), as a function of fundamental Planck scale (M_D) for $n = 2$, where n is the number of extra spatial dimensions. The 95% CL expected (dotted) and observed (solid) lower limits (right) on M_D as a function of n in the ADD model. The results are also compared to earlier ones obtained by the CMS Collaboration with data corresponding to an integrated luminosity of 19.7 fb^{-1} at a centre-of-mass energy of 8 TeV [10] (blue points).

Table 7: Upper limits on the signal production cross section in the ADD model and lower limits on M_D , both as functions of the number of extra spatial dimensions (n).

n	Observed (expected) cross section exclusion [pb]	Observed (expected) M_D exclusions [TeV]
2	0.28 (0.22)	9.9 (10.5)
3	0.18 (0.15)	7.5 (7.8)
4	0.15 (0.13)	6.3 (6.5)
5	0.13 (0.11)	5.7 (6.0)
6	0.13 (0.10)	5.3 (5.4)

7 Summary

A search for dark matter (DM) particles, invisible decays of a standard-model-like (SM-like) Higgs boson, and extra spatial dimensions is presented using events with one or more energetic jets and large missing transverse momentum in proton-proton collisions recorded at $\sqrt{s} = 13$ TeV, using a sample of data corresponding to an integrated luminosity of 35.9 fb^{-1} . Events are categorized based on whether jets are produced directly in hard scattering as initial-state radiation or originate from merged quarks from a decay of a highly Lorentz-boosted W or Z boson. No excess of events is observed compared to the SM background expectations in either of these two categories.

Limits are computed on the DM production cross section using simplified models in which DM production is mediated by spin-1 and spin-0 particles. Vector and axial-vector (pseudoscalar) mediators with masses up to 1.8 (0.4) TeV are excluded at 95% confidence level. Similarly, limits are also presented for the parameters of the fermion portal DM model and an exclusion up to 1.4 TeV on the mediator mass is observed at 95% confidence level. The first limits on the DM production at a particle collider in the nonthermal DM model are obtained and presented in the coupling strength plane. Furthermore, an observed (expected) 95% confidence level upper limit of 0.53 (0.40) is set for the invisible branching fraction of an SM-like 125 GeV Higgs boson, assuming the SM production cross section. Lower limits are also computed on the fundamental Planck scale M_D in the context of the Arkani-Hamed, Dimopoulos, and Dvali model with large extra spatial dimensions, which varies from 9.9 TeV for $n = 2$ to 5.3 TeV for $n = 6$ at 95% confidence level, where n is the number of extra spatial dimensions. These limits provide the most stringent direct constraints on the fundamental Planck scale to date.

Acknowledgments

We congratulate our colleagues in the CERN accelerator departments for the excellent performance of the LHC and thank the technical and administrative staffs at CERN and at other CMS institutes for their contributions to the success of the CMS effort. In addition, we gratefully acknowledge the computing centres and personnel of the Worldwide LHC Computing Grid for delivering so effectively the computing infrastructure essential to our analyses. Finally, we acknowledge the enduring support for the construction and operation of the LHC and the CMS detector provided by the following funding agencies: BMWFW and FWF (Austria); FNRS and FWO (Belgium); CNPq, CAPES, FAPERJ, and FAPESP (Brazil); MES (Bulgaria); CERN; CAS, MoST, and NSFC (China); COLCIENCIAS (Colombia); MSES and CSF (Croatia); RPF (Cyprus); SENESCYT (Ecuador); MoER, ERC IUT, and ERDF (Estonia); Academy of Finland, MEC, and HIP (Finland); CEA and CNRS/IN2P3 (France); BMBF, DFG, and HGF (Ger-

many); GSRT (Greece); OTKA and NIH (Hungary); DAE and DST (India); IPM (Iran); SFI (Ireland); INFN (Italy); MSIP and NRF (Republic of Korea); LAS (Lithuania); MOE and UM (Malaysia); BUAP, CINVESTAV, CONACYT, LNS, SEP, and UASLP-FAI (Mexico); MBIE (New Zealand); PAEC (Pakistan); MSHE and NSC (Poland); FCT (Portugal); JINR (Dubna); MON, RosAtom, RAS, RFBR and RAEP (Russia); MESTD (Serbia); SEIDI, CPAN, PCTI and FEDER (Spain); Swiss Funding Agencies (Switzerland); MST (Taipei); ThEPCenter, IPST, STAR, and NSTDA (Thailand); TUBITAK and TAEK (Turkey); NASU and SFFR (Ukraine); STFC (United Kingdom); DOE and NSF (USA).

Individuals have received support from the Marie-Curie programme and the European Research Council and Horizon 2020 Grant, contract No. 675440 (European Union); the Leventis Foundation; the A. P. Sloan Foundation; the Alexander von Humboldt Foundation; the Belgian Federal Science Policy Office; the Fonds pour la Formation à la Recherche dans l'Industrie et dans l'Agriculture (FRIA-Belgium); the Agentschap voor Innovatie door Wetenschap en Technologie (IWT-Belgium); the Ministry of Education, Youth and Sports (MEYS) of the Czech Republic; the Council of Science and Industrial Research, India; the HOMING PLUS programme of the Foundation for Polish Science, cofinanced from European Union, Regional Development Fund, the Mobility Plus programme of the Ministry of Science and Higher Education, the National Science Center (Poland), contracts Harmonia 2014/14/M/ST2/00428, Opus 2014/13/B/ST2/02543, 2014/15/B/ST2/03998, and 2015/19/B/ST2/02861, Sonata-bis 2012/07/E/ST2/01406; the National Priorities Research Program by Qatar National Research Fund; the Programa Clarín-COFUND del Principado de Asturias; the Thalís and Aristeia programmes cofinanced by EU-ESF and the Greek NSRF; the Rachadapisek Sompot Fund for Postdoctoral Fellowship, Chulalongkorn University and the Chulalongkorn Academic into Its 2nd Century Project Advancement Project (Thailand); and the Welch Foundation, contract C-1845.

References

- [1] G. Bertone, D. Hooper, and J. Silk, "Particle dark matter: evidence, candidates and constraints", *Phys. Rept.* **405** (2005) 279, doi:10.1016/j.physrep.2004.08.031, arXiv:hep-ph/0404175.
- [2] J. L. Feng, "Dark matter candidates from particle physics and methods of detection", *Ann. Rev. Astron. Astrophys.* **48** (2010) 495, doi:10.1146/annurev-astro-082708-101659, arXiv:1003.0904.
- [3] T. A. Porter, R. P. Johnson, and P. W. Graham, "Dark matter searches with astroparticle data", *Ann. Rev. Astron. Astrophys.* **49** (2011) 155, doi:10.1146/annurev-astro-081710-102528, arXiv:1104.2836.
- [4] N. Arkani-Hamed, S. Dimopoulos, and G. Dvali, "The hierarchy problem and new dimensions at a millimeter", *Phys. Lett. B* **429** (1998) 263, doi:10.1016/S0370-2693(98)00466-3, arXiv:hep-ph/9803315.
- [5] N. Arkani-Hamed, S. Dimopoulos, and G. R. Dvali, "Phenomenology, astrophysics and cosmology of theories with submillimeter dimensions and TeV scale quantum gravity", *Phys. Rev. D* **59** (1999) 086004, doi:10.1103/PhysRevD.59.086004, arXiv:hep-ph/9807344.
- [6] I. Antoniadis, K. Benakli, and M. Quiros, "Direct collider signatures of large extra dimensions", *Phys. Lett. B* **460** (1999) 176, doi:10.1016/S0370-2693(99)00764-9, arXiv:hep-ph/9905311.

- [7] G. Giudice, R. Rattazzi, and J. Wells, “Quantum gravity and extra dimensions at high-energy colliders”, *Nucl. Phys. B* **544** (1999) 3, doi:10.1016/S0550-3213(99)00044-9, arXiv:hep-ph/9811291.
- [8] E. A. Mirabelli, M. Perelstein, and M. E. Peskin, “Collider signatures of new large space dimensions”, *Phys. Rev. Lett.* **82** (1999) 2236, doi:10.1103/PhysRevLett.82.2236, arXiv:hep-ph/9811337.
- [9] ATLAS Collaboration, “Search for dark matter in events with a hadronically decaying W or Z boson and missing transverse momentum in pp collisions at $\sqrt{s} = 8$ TeV with the ATLAS detector”, *Phys. Rev. Lett.* **112** (2014) 041802, doi:10.1103/PhysRevLett.112.041802, arXiv:1309.4017.
- [10] CMS Collaboration, “Search for dark matter, extra dimensions, and unparticles in monojet events in proton-proton collisions at $\sqrt{s} = 8$ TeV”, *Eur. Phys. J. C* **75** (2015) 235, doi:10.1140/epjc/s10052-015-3451-4, arXiv:1408.3583.
- [11] ATLAS Collaboration, “Search for new phenomena in final states with an energetic jet and large missing transverse momentum in pp collisions at $\sqrt{s} = 8$ TeV with the ATLAS detector”, *Eur. Phys. J. C* **75** (2015) 299, doi:10.1140/epjc/s10052-015-3517-3, arXiv:1502.01518. [Erratum: doi:10.1140/epjc/s10052-015-3639-7].
- [12] CMS Collaboration, “Search for dark matter in proton-proton collisions at 8 TeV with missing transverse momentum and vector boson tagged jets”, *JHEP* **12** (2016) 083, doi:10.1007/JHEP12(2016)083, arXiv:1607.05764.
- [13] ATLAS Collaboration, “Search for new phenomena in final states with an energetic jet and large missing transverse momentum in pp collisions at $\sqrt{s} = 13$ TeV using the ATLAS detector”, *Phys. Rev. D* **94** (2016) 032005, doi:10.1103/PhysRevD.94.032005, arXiv:1604.07773.
- [14] CMS Collaboration, “Search for dark matter produced with an energetic jet or a hadronically decaying W or Z boson at $\sqrt{s} = 13$ TeV”, *JHEP* **07** (2017) 014, doi:10.1007/JHEP07(2017)014, arXiv:1703.01651.
- [15] ATLAS Collaboration, “Search for dark matter and other new phenomena in events with an energetic jet and large missing transverse momentum using the ATLAS detector”, *JHEP* **01** (2018) 126, doi:/10.1007/JHEP01(2018)126, arXiv:1711.03301.
- [16] J. M. Lindert et al., “Precise predictions for V+jets dark matter backgrounds”, *Eur. Phys. J. C* **77** (2017) 829, doi:10.1140/epjc/s10052-017-5389-1, arXiv:1705.04664.
- [17] G. Busoni, A. De Simone, E. Morgante, and A. Riotto, “On the validity of the effective field theory for dark matter searches at the LHC”, *Phys. Lett. B* **728** (2014) 412, doi:10.1016/j.physletb.2013.11.069, arXiv:1307.2253.
- [18] O. Buchmueller, M. J. Dolan, and C. McCabe, “Beyond effective field theory for dark matter searches at the LHC”, *JHEP* **01** (2014) 025, doi:10.1007/JHEP01(2014)025, arXiv:1308.6799.
- [19] O. Buchmueller, M. J. Dolan, S. A. Malik, and C. McCabe, “Characterising dark matter searches at colliders and direct detection experiments: vector mediators”, *JHEP* **01** (2015) 037, doi:10.1007/JHEP01(2015)037, arXiv:1407.8257.

- [20] Y. Bai and J. Berger, “Fermion portal dark matter”, *JHEP* **11** (2013) 171, doi:10.1007/JHEP11(2013)171, arXiv:1308.0612.
- [21] B. Dutta, Y. Gao, and T. Kamon, “Probing light nonthermal dark matter at the LHC”, *Phys. Rev. D* **89** (2014) 096009, doi:10.1103/PhysRevD.89.096009, arXiv:1401.1825.
- [22] R. Allahverdi and B. Dutta, “Natural GeV dark matter and the baryon-dark matter coincidence puzzle”, *Phys. Rev. D* **88** (2013) 023525, doi:10.1103/PhysRevD.88.023525, arXiv:1304.0711.
- [23] J. Alwall, P. C. Schuster, and N. Toro, “Simplified models for a first characterization of new physics at the LHC”, *Phys. Rev. D* **79** (2009) 075020, doi:10.1103/PhysRevD.79.075020, arXiv:0810.3921.
- [24] J. Goodman and W. Shepherd, “LHC bounds on UV-complete models of dark matter”, (2011). arXiv:1111.2359.
- [25] LHC New Physics Working Group Collaboration, “Simplified models for LHC new physics searches”, *J. Phys. G* **39** (2012) 105005, doi:10.1088/0954-3899/39/10/105005, arXiv:1105.2838.
- [26] H. An, X. Ji, and L.-T. Wang, “Light dark matter and Z' dark force at colliders”, *JHEP* **07** (2012) 182, doi:10.1007/JHEP07(2012)182, arXiv:1202.2894.
- [27] H. An, R. Huo, and L.-T. Wang, “Searching for low mass dark portal at the LHC”, *Phys. Dark Univ.* **2** (2013) 50, doi:10.1016/j.dark.2013.03.002, arXiv:1212.2221.
- [28] A. DiFranzo, K. I. Nagao, A. Rajaraman, and T. M. P. Tait, “Simplified models for dark matter interacting with quarks”, *JHEP* **11** (2013) 014, doi:10.1007/JHEP11(2013)014, arXiv:1308.2679. [Erratum: doi:10.1007/JHEP01(2014)162].
- [29] Y. Bai and J. Berger, “Lepton portal dark matter”, *JHEP* **08** (2014) 153, doi:10.1007/JHEP08(2014)153, arXiv:1402.6696.
- [30] H. An, L.-T. Wang, and H. Zhang, “Dark matter with t -channel mediator: a simple step beyond contact interaction”, *Phys. Rev. D* **89** (2014) 115014, doi:10.1103/PhysRevD.89.115014, arXiv:1308.0592.
- [31] J. Abdallah et al., “Simplified models for dark matter and missing energy searches at the LHC”, (2014). arXiv:1409.2893.
- [32] S. A. Malik et al., “Interplay and characterization of dark matter searches at colliders and in direct detection experiments”, *Phys. Dark Univ.* **9-10** (2015) 51, doi:10.1016/j.dark.2015.03.003, arXiv:1409.4075.
- [33] P. Harris, V. V. Khoze, M. Spannowsky, and C. Williams, “Constraining dark sectors at colliders: Beyond the effective theory approach”, *Phys. Rev. D* **91** (2015) 055009, doi:10.1103/PhysRevD.91.055009, arXiv:1411.0535.
- [34] M. R. Buckley, D. Feld, and D. Goncalves, “Scalar simplified models for dark matter”, *Phys. Rev. D* **91** (2015) 015017, doi:10.1103/PhysRevD.91.015017, arXiv:1410.6497.

- [35] U. Haisch and E. Re, “Simplified dark matter top-quark interactions at the LHC”, *JHEP* **06** (2015) 078, doi:10.1007/JHEP06(2015)078, arXiv:1503.00691.
- [36] P. Harris, V. V. Khoze, M. Spannowsky, and C. Williams, “Closing up on dark sectors at colliders: from 14 to 100 TeV”, *Phys. Rev. D* **93** (2016) 054030, doi:10.1103/PhysRevD.93.054030, arXiv:1509.02904.
- [37] L. M. Carpenter et al., “Collider searches for dark matter in events with a Z boson and missing energy”, *Phys. Rev. D* **87** (2013) 074005, doi:10.1103/PhysRevD.87.074005, arXiv:1212.3352.
- [38] N. F. Bell et al., “Searching for dark matter at the LHC with a mono-Z”, *Phys. Rev. D* **86** (2012) 096011, doi:10.1103/PhysRevD.86.096011, arXiv:1209.0231.
- [39] ATLAS Collaboration, “Constraints on new phenomena via Higgs boson couplings and invisible decays with the ATLAS detector”, *JHEP* **11** (2015) 206, doi:10.1007/JHEP11(2015)206, arXiv:1509.00672.
- [40] CMS Collaboration, “Searches for invisible decays of the Higgs boson in pp collisions at $\sqrt{s} = 7, 8, \text{ and } 13 \text{ TeV}$ ”, *JHEP* **02** (2017) 135, doi:10.1007/JHEP02(2017)135, arXiv:1610.09218.
- [41] ATLAS Collaboration, “Observation of a new particle in the search for the Standard Model Higgs boson with the ATLAS detector at the LHC”, *Phys. Lett. B* **716** (2012) 1, doi:10.1016/j.physletb.2012.08.020, arXiv:1207.7214.
- [42] CMS Collaboration, “Observation of a new boson at a mass of 125 GeV with the CMS experiment at the LHC”, *Phys. Lett. B* **716** (2012) 30, doi:10.1016/j.physletb.2012.08.021, arXiv:1207.7235.
- [43] CMS Collaboration, “Observation of a new boson with mass near 125 GeV in pp collisions at $\sqrt{s} = 7 \text{ and } 8 \text{ TeV}$ ”, *JHEP* **06** (2013) 081, doi:10.1007/JHEP06(2013)081, arXiv:1303.4571.
- [44] CMS Collaboration, “The CMS experiment at the CERN LHC”, *JINST* **3** (2008) S08004, doi:10.1088/1748-0221/3/08/S08004.
- [45] CMS Collaboration, “Particle-flow reconstruction and global event description with the CMS detector”, *JINST* **12** (2017) P10003, doi:10.1088/1748-0221/12/10/P10003, arXiv:1706.04965.
- [46] M. Cacciari, G. P. Salam, and G. Soyez, “The anti- k_t jet clustering algorithm”, *JHEP* **04** (2008) 063, doi:10.1088/1126-6708/2008/04/063, arXiv:0802.1189.
- [47] M. Cacciari, G. P. Salam, and G. Soyez, “FastJet user manual”, *Eur. Phys. J. C* **72** (2012) 1896, doi:10.1140/epjc/s10052-012-1896-2, arXiv:1111.6097.
- [48] CMS Collaboration, “Jet energy scale and resolution in the CMS experiment in pp collisions at 8 TeV”, *JINST* **12** (2017) P02014, doi:10.1088/1748-0221/12/02/P02014, arXiv:1607.03663.
- [49] CMS Collaboration, “Performance of missing energy reconstruction in 13 TeV pp collision data using the CMS detector”, CMS Physics Analysis Summary CMS-PAS-JME-16-004.

-
- [50] CMS Collaboration, “Performance of the CMS missing transverse momentum reconstruction in pp data at $\sqrt{s} = 8 \text{ TeV}$ ”, *JINST* **10** (2015) P02006, doi:10.1088/1748-0221/10/02/P02006, arXiv:1411.0511.
- [51] CMS Collaboration, “Performance of CMS muon reconstruction in pp collision events at $\sqrt{s} = 7 \text{ TeV}$ ”, *JINST* **7** (2012) P10002, doi:10.1088/1748-0221/7/10/P10002, arXiv:1206.4071.
- [52] CMS Collaboration, “Performance of electron reconstruction and selection with the CMS detector in proton-proton collisions at $\sqrt{s} = 8 \text{ TeV}$ ”, *JINST* **10** (2015) P06005, doi:10.1088/1748-0221/10/06/P06005, arXiv:1502.02701.
- [53] CMS Collaboration, “Description and performance of track and primary-vertex reconstruction with the CMS tracker”, *JINST* **9** (2014) P10009, doi:10.1088/1748-0221/9/10/P10009, arXiv:1405.6569.
- [54] CMS Collaboration, “Performance of photon reconstruction and identification with the CMS detector in proton-proton collisions at $\sqrt{s} = 8 \text{ TeV}$ ”, *JINST* **10** (2015) P08010, doi:10.1088/1748-0221/10/08/P08010, arXiv:1502.02702.
- [55] CMS Collaboration, “Reconstruction and identification of τ lepton decays to hadrons and ν_τ at CMS”, *JINST* **11** (2016) P01019, doi:10.1088/1748-0221/11/01/P01019, arXiv:1510.07488.
- [56] J. Alwall et al., “The automated computation of tree-level and next-to-leading order differential cross sections, and their matching to parton shower simulations”, *JHEP* **07** (2014) 079, doi:10.1007/JHEP07(2014)079, arXiv:1405.0301.
- [57] C. Oleari, “The POWHEG-BOX”, *Nucl. Phys. Proc. Suppl.* **205-206** (2010) 36, doi:10.1016/j.nuclphysbps.2010.08.016, arXiv:1007.3893.
- [58] S. Alioli, P. Nason, C. Oleari, and E. Re, “NLO single-top production matched with shower in POWHEG: s - and t -channel contributions”, *JHEP* **09** (2009) 111, doi:10.1088/1126-6708/2009/09/111, arXiv:0907.4076. [Erratum: doi:10.1007/JHEP02(2010)011].
- [59] T. Sjöstrand et al., “An Introduction to PYTHIA 8.2”, *Comput. Phys. Commun.* **191** (2015) 159, doi:10.1016/j.cpc.2015.01.024, arXiv:1410.3012.
- [60] M. Backović et al., “Higher-order QCD predictions for dark matter production at the LHC in simplified models with s -channel mediators”, *Eur. Phys. J. C* **75** (2015) 482, doi:10.1140/epjc/s10052-015-3700-6, arXiv:1508.05327.
- [61] O. Mattelaer and E. Vryonidou, “Dark matter production through loop-induced processes at the LHC: the s -channel mediator case”, *Eur. Phys. J. C* **75** (2015) 436, doi:10.1140/epjc/s10052-015-3665-5, arXiv:1508.00564.
- [62] S. Alioli, P. Nason, C. Oleari, and E. Re, “NLO Higgs boson production via gluon fusion matched with shower in POWHEG”, *JHEP* **04** (2009) 002, doi:10.1088/1126-6708/2009/04/002, arXiv:0812.0578.
- [63] P. Nason and C. Oleari, “NLO Higgs boson production via vector-boson fusion matched with shower in POWHEG”, *JHEP* **02** (2010) 037, doi:10.1007/JHEP02(2010)037, arXiv:0911.5299.

- [64] I. Anderson et al., “Constraining anomalous HVV interactions at proton and lepton colliders”, *Phys. Rev. D* **89** (2014) 035007, doi:10.1103/PhysRevD.89.035007, arXiv:1309.4819.
- [65] CMS Collaboration, “Event generator tunes obtained from underlying event and multiparton scattering measurements”, *Eur. Phys. J. C* **76** (2016) 155, doi:10.1140/epjc/s10052-016-3988-x, arXiv:1512.00815.
- [66] M. L. Mangano, M. Moretti, F. Piccinini, and M. Treccani, “Matching matrix elements and shower evolution for top-quark production in hadronic collisions”, *JHEP* **01** (2007) 013, doi:10.1088/1126-6708/2007/01/013, arXiv:hep-ph/0611129.
- [67] R. Frederix and S. Frixione, “Merging meets matching in MC@NLO”, *JHEP* **12** (2012) 061, doi:10.1007/JHEP12(2012)061, arXiv:1209.6215.
- [68] NNPDF Collaboration, “Parton distributions for the LHC Run II”, *JHEP* **04** (2015) 040, doi:10.1007/JHEP04(2015)040, arXiv:1410.8849.
- [69] GEANT4 Collaboration, “GEANT4—a simulation toolkit”, *Nucl. Instrum. Meth. A* **506** (2003) 250, doi:10.1016/S0168-9002(03)01368-8.
- [70] CMS Collaboration, “CMS luminosity measurements for the 2016 data taking period”, Physics Analysis Summary CMS-PAS-LUM-17-001.
- [71] CMS Collaboration, “Identification of b-quark jets with the CMS experiment”, *JINST* **8** (2013) P04013, doi:10.1088/1748-0221/8/04/P04013, arXiv:1211.4462.
- [72] CMS Collaboration, “Identification of b quark jets at the CMS experiment in the LHC Run 2”, CMS Physics Analysis Summary CMS-PAS-BTV-15-001.
- [73] CMS Collaboration, “Jet algorithms performance in 13 TeV data”, CMS Physics Analysis Summary CMS-PAS-JME-16-003.
- [74] S. D. Ellis, C. K. Vermilion, and J. R. Walsh, “Recombination algorithms and jet substructure: Pruning as a tool for heavy particle searches”, *Phys. Rev. D* **81** (2010) 094023, doi:10.1103/PhysRevD.81.094023, arXiv:0912.0033.
- [75] S. D. Ellis, C. K. Vermilion, and J. R. Walsh, “Techniques for improved heavy particle searches with jet substructure”, *Phys. Rev. D* **80** (2009) 051501, doi:10.1103/PhysRevD.80.051501, arXiv:0903.5081.
- [76] Yu. L. Dokshitzer, G. D. Leder, S. Moretti, and B. R. Webber, “Better jet clustering algorithms”, *JHEP* **08** (1997) 001, doi:10.1088/1126-6708/1997/08/001, arXiv:hep-ph/9707323.
- [77] J. Thaler and K. Van Tilburg, “Identifying boosted objects with N-subjettiness”, *JHEP* **03** (2011) 015, doi:10.1007/JHEP03(2011)015, arXiv:1011.2268.
- [78] A. Denner, S. Dittmaier, T. Kasprzik, and A. Muck, “Electroweak corrections to W+jet hadroproduction including leptonic W-boson decays”, *JHEP* **08** (2009) 075, doi:10.1088/1126-6708/2009/08/075, arXiv:0906.1656.
- [79] A. Denner, S. Dittmaier, T. Kasprzik, and A. Muck, “Electroweak corrections to dilepton+jet production at hadron colliders”, *JHEP* **06** (2011) 069, doi:10.1007/JHEP06(2011)069, arXiv:1103.0914.

- [80] A. Denner, S. Dittmaier, T. Kasprzik, and A. Maeck, “Electroweak corrections to monojet production at the LHC”, *Eur. Phys. J. C* **73** (2013) 2297, doi:10.1140/epjc/s10052-013-2297-x, arXiv:1211.5078.
- [81] J. H. Kuhn, A. Kulesza, S. Pozzorini, and M. Schulze, “Electroweak corrections to hadronic photon production at large transverse momenta”, *JHEP* **03** (2006) 059, doi:10.1088/1126-6708/2006/03/059, arXiv:hep-ph/0508253.
- [82] S. Kallweit et al., “NLO electroweak automation and precise predictions for W+multijet production at the LHC”, *JHEP* **04** (2015) 012, doi:10.1007/JHEP04(2015)012, arXiv:1412.5157.
- [83] S. Kallweit et al., “NLO QCD+EW predictions for V+jets including off-shell vector-boson decays and multijet merging”, *JHEP* **04** (2016) 021, doi:10.1007/JHEP04(2016)021, arXiv:1511.08692.
- [84] CMS Collaboration, “Search for new physics with jets and missing transverse momentum in pp collisions at $\sqrt{s} = 7$ TeV”, *JHEP* **08** (2011) 155, doi:10.1007/JHEP08(2011)155, arXiv:1106.4503.
- [85] J. H. Kuhn, A. Kulesza, S. Pozzorini, and M. Schulze, “Logarithmic electroweak corrections to hadronic Z+1 jet production at large transverse momentum”, *Phys. Lett. B* **609** (2005) 277, doi:10.1016/j.physletb.2005.01.059, arXiv:hep-ph/0408308.
- [86] J. H. Kuhn, A. Kulesza, S. Pozzorini, and M. Schulze, “One-loop weak corrections to hadronic production of Z bosons at large transverse momenta”, *Nucl. Phys. B* **727** (2005) 368, doi:10.1016/j.nuclphysb.2005.08.019, arXiv:hep-ph/0507178.
- [87] J. H. Kuhn, A. Kulesza, S. Pozzorini, and M. Schulze, “Electroweak corrections to hadronic production of W bosons at large transverse momenta”, *Nucl. Phys. B* **797** (2008) 27, doi:10.1016/j.nuclphysb.2007.12.029, arXiv:0708.0476.
- [88] CMS Collaboration, “Measurement of differential cross sections for top quark pair production using the lepton+jets final state in proton-proton collisions at 13 TeV”, *Phys. Rev. D* **95** (2017) 092001, doi:10.1103/PhysRevD.95.092001, arXiv:1610.04191.
- [89] CMS Collaboration, “Measurement of the top quark pair production cross section in proton-proton collisions at $\sqrt{s} = 13$ TeV”, *Phys. Rev. Lett.* **116** (2016) 052002, doi:10.1103/PhysRevLett.116.052002, arXiv:1510.05302.
- [90] CMS Collaboration, “Measurement of the ZZ production cross section and $Z \rightarrow \ell^+ \ell^- \ell'^+ \ell'^-$ branching fraction in pp collisions at $\sqrt{s} = 13$ TeV”, *Phys. Lett. B* **763** (2016) 280, doi:10.1016/j.physletb.2016.10.054, arXiv:1607.08834.
- [91] CMS Collaboration, “Measurement of the WZ production cross section in pp collisions at $\sqrt{s} = 13$ TeV”, *Phys. Lett. B* **766** (2017) 268, doi:10.1016/j.physletb.2017.01.011, arXiv:1607.06943.
- [92] CMS Collaboration, “Simplified likelihood for the re-interpretation of public CMS results”, CMS Note CMS-NOTE-2017-001.
- [93] D. Abercrombie et al., “Dark matter benchmark models for early LHC Run-2 searches: Report of the ATLAS/CMS dark matter forum”, (2015). arXiv:1507.00966.

- [94] T. Junk, “Confidence level computation for combining searches with small statistics”, *Nucl. Instrum. Meth. A* **434** (1999) 435, doi:10.1016/S0168-9002(99)00498-2, arXiv:hep-ex/9902006.
- [95] A. L. Read, “Presentation of search results: the CLs technique”, *J. Phys. G* **28** (2002) 2693, doi:10.1088/0954-3899/28/10/313.
- [96] G. Cowan, K. Cranmer, E. Gross, and O. Vitells, “Asymptotic formulae for likelihood-based tests of new physics”, *Eur. Phys. J. C* **71** (2011) 1554, doi:10.1140/epjc/s10052-011-1554-0, arXiv:1007.1727. [Erratum: doi:10.1140/epjc/s10052-013-2501-z].
- [97] Planck Collaboration, “Planck 2015 results. XIII. Cosmological parameters”, *Astron. Astrophys.* **594** (2016) A13, doi:10.1051/0004-6361/201525830, arXiv:1502.01589.
- [98] M. Backović, K. Kong, and M. McCaskey, “MadDM v.1.0: Computation of dark matter relic abundance using MadGraph5”, *Phys. Dark Univ.* **5-6** (2014) 18, doi:10.1016/j.dark.2014.04.001, arXiv:1308.4955.
- [99] Planck Collaboration, “Planck 2013 results. XVI. Cosmological parameters”, *Astron. Astrophys.* **571** (2014) A16, doi:10.1051/0004-6361/201321591, arXiv:1303.5076.
- [100] G. Busoni et al., “Recommendations on presenting LHC searches for missing transverse energy signals using simplified s-channel models of dark matter”, (2016). arXiv:1603.04156.
- [101] Fermi-LAT Collaboration, “Searching for dark matter annihilation from Milky Way dwarf spheroidal galaxies with six years of Fermi Large Area Telescope data”, *Phys. Rev. Lett.* **115** (2015) 231301, doi:10.1103/PhysRevLett.115.231301, arXiv:1503.02641.
- [102] SuperCDMS Collaboration, “New results from the search for low-mass weakly interacting massive particles with the CDMS low ionization threshold experiment”, *Phys. Rev. Lett.* **116** (2016) 071301, doi:10.1103/PhysRevLett.116.071301, arXiv:1509.02448.
- [103] LUX Collaboration, “Results from a search for dark matter in the complete LUX exposure”, *Phys. Rev. Lett.* **118** (2017) 021303, doi:10.1103/PhysRevLett.118.021303, arXiv:1608.07648.
- [104] XENON Collaboration, “First dark matter search results from the XENON1T experiment”, *Phys. Rev. Lett.* **119** (2017) 181301, doi:10.1103/PhysRevLett.119.181301, arXiv:1705.06655.
- [105] PandaX-II Collaboration, “Dark matter results from 54-ton-day exposure of PandaX-II experiment”, *Phys. Rev. Lett.* **119** (2017) 181302, doi:10.1103/PhysRevLett.119.181302, arXiv:1708.06917.
- [106] CRESST Collaboration, “Results on light dark matter particles with a low-threshold CRESST-II detector”, *Eur. Phys. J. C* **76** (2016) 25, doi:10.1140/epjc/s10052-016-3877-3, arXiv:1509.01515.

- [107] E. Behnke et al., “Final results of the PICASSO dark matter search experiment”, *Astropart. Phys.* **90** (2017) 85, doi:10.1016/j.astropartphys.2017.02.005, arXiv:1611.01499.
- [108] PICO Collaboration, “Dark matter search results from the PICO-60 CF₃I bubble chamber”, *Phys. Rev. D* **93** (2016) 052014, doi:10.1103/PhysRevD.93.052014, arXiv:1510.07754.
- [109] IceCube Collaboration, “Improved limits on dark matter annihilation in the Sun with the 79-string IceCube detector and implications for supersymmetry”, *JCAP* **04** (2016) 022, doi:10.1088/1475-7516/2016/04/022, arXiv:1601.00653.
- [110] Super-Kamiokande Collaboration, “Search for neutrinos from annihilation of captured low-mass dark matter particles in the Sun by Super-Kamiokande”, *Phys. Rev. Lett.* **114** (2015) 141301, doi:10.1103/PhysRevLett.114.141301, arXiv:1503.04858.
- [111] U. Haisch, F. Kahlhoefer, and J. Unwin, “The impact of heavy-quark loops on LHC dark matter searches”, *JHEP* **07** (2013) 125, doi:10.1007/JHEP07(2013)125, arXiv:1208.4605.
- [112] A. Berlin, D. Hooper, and S. D. McDermott, “Simplified dark matter models for the galactic center gamma-ray excess”, *Phys. Rev. D* **89** (2014) 115022, doi:10.1103/PhysRevD.89.115022, arXiv:1404.0022.
- [113] LHC Higgs Cross Section Working Group Collaboration, “Handbook of LHC Higgs cross sections: 3. Higgs properties”, (2013). arXiv:1307.1347.

A Additional material

Another important cross-check of the application of p_T -dependent NLO QCD and EW corrections is represented by the agreement between data and simulation in the ratio of Z+jets events to both γ +jets events and W+jets events in the control samples as a function of boson p_T .

Figure 19 shows the ratio between $Z(\mu\mu)$ +jets and γ +jets, and the ratio of $Z(\mu\mu)$ +jets and $W(\mu\nu)$ +jets events as a function of the boson p_T , for the monojet category. While we do not explicitly use a $W(\mu\nu)$ +jets/ γ +jets constraint in the analysis, the two cross sections are connected through the Z+jets/ γ +jets and Z+jets/W+jets constraints. Therefore, it is instructive to examine the data-to-simulation comparison for the $W(\mu\nu)$ +jets/ γ +jets ratio. This is shown in the same figure. Good agreement is observed between data and simulation after the application of NLO corrections.

The correlations between the predicted background yields across all the p_T^{miss} bins in the two signal regions are shown in Figs. 20 and 21. These results can be used with the simplified likelihood approach detailed in Ref. [92] for reinterpretations in terms of models not studied in this paper.

To allow for a direct comparison with the results of Ref. [14] for simplified DM models, the results are presented for scalar mediators allowing for vector boson couplings simulated at LO in QCD, as shown in Fig. 22. Similarly, results for spin-1 mediators are also presented in Fig. 23, where the mono-V signal is simulated at LO in QCD. The comparison of MC generators are also provided in Table 8.

Table 8: Monte Carlo generators and perturbative order in QCD used for simulating various signal processes studied in this work, and in Ref. [14]

Process	Monte Carlo generator (Perturbative order in QCD) Ref. [14]	Monte Carlo generator (Perturbative order in QCD) this work
Monojet (spin-1 med.)	POWHEG 2.0 (NLO)	MADGRAPH5_aMC@NLO 2.2.3 (NLO)
Monojet (spin-0 med.)	POWHEG 2.0 (LO)	MADGRAPH5_aMC@NLO 2.2.3 (NLO)
mono-V (spin-1 med.)	MADGRAPH5_aMC@NLO 2.2.3 (LO)	MADGRAPH5_aMC@NLO 2.2.3 (NLO)
mono-V (spin-0 med.)	JHUGENERATOR 5.2.5	Not used

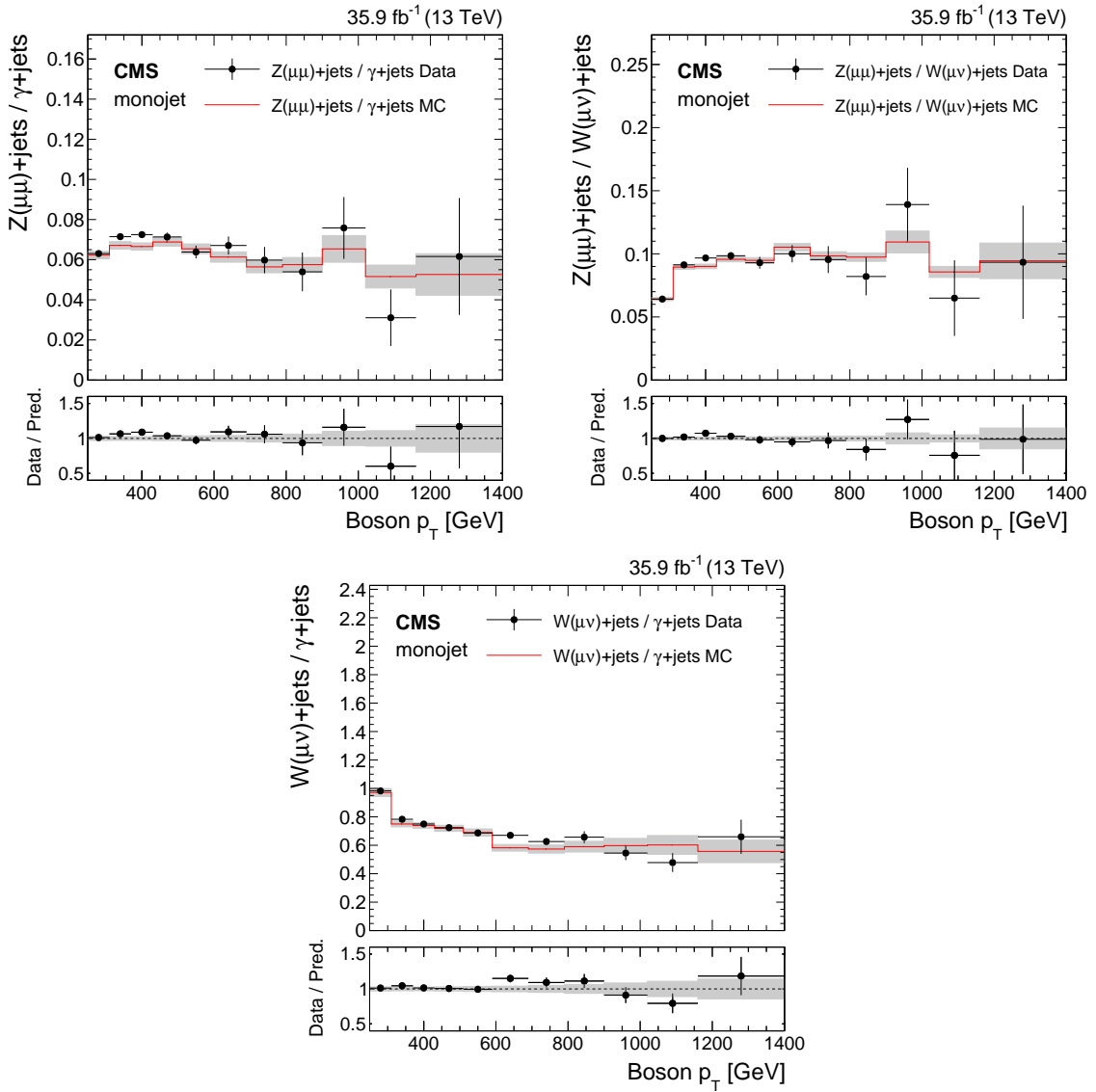


Figure 19: Comparison between data and Monte Carlo simulation of the $Z(\mu\mu)/\gamma$ +jets, $Z(\mu\mu)/W(\mu\nu)$ and $W(\mu\nu)/\gamma$ +jets ratios, as a function of boson p_T , in the monojet category. In the ratio panel, ratios of data with the pre-fit background prediction are shown. The gray bands include both the pre-fit systematic uncertainties and the statistical uncertainty in the simulation.

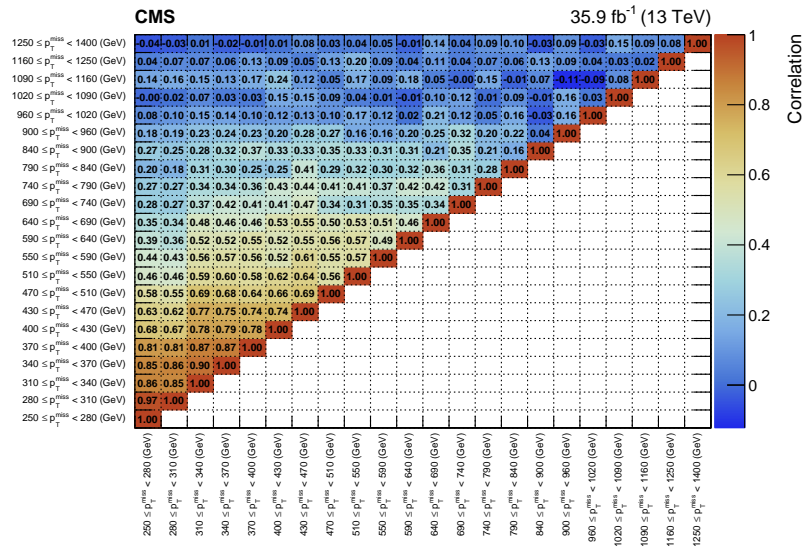


Figure 20: Correlations between the predicted background yields in all the E_T^{miss} bins of the monojet signal region. The boundaries of the E_T^{miss} bins, expressed in GeV, are shown at the bottom and on the left.

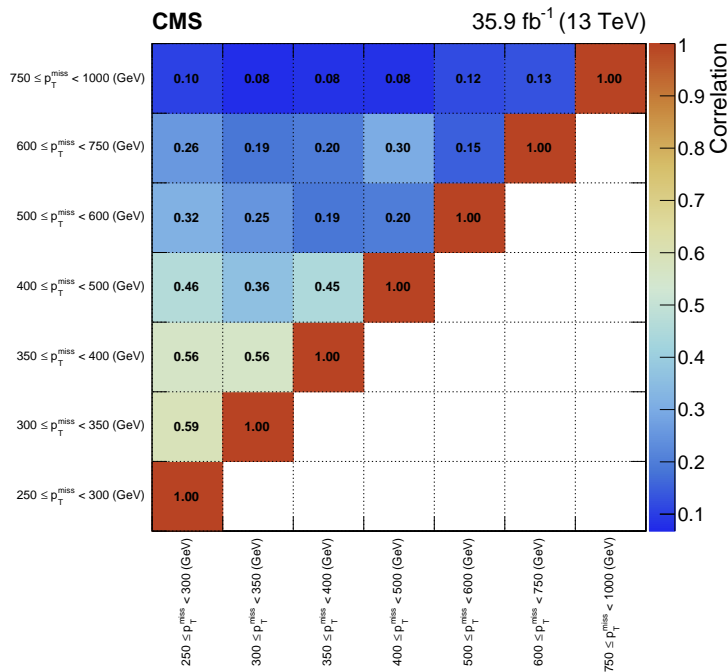


Figure 21: Correlations between the predicted background yields in all the E_T^{miss} bins of the mono-V signal region. The boundaries of the E_T^{miss} bins, expressed in GeV, are shown at the bottom and on the left.

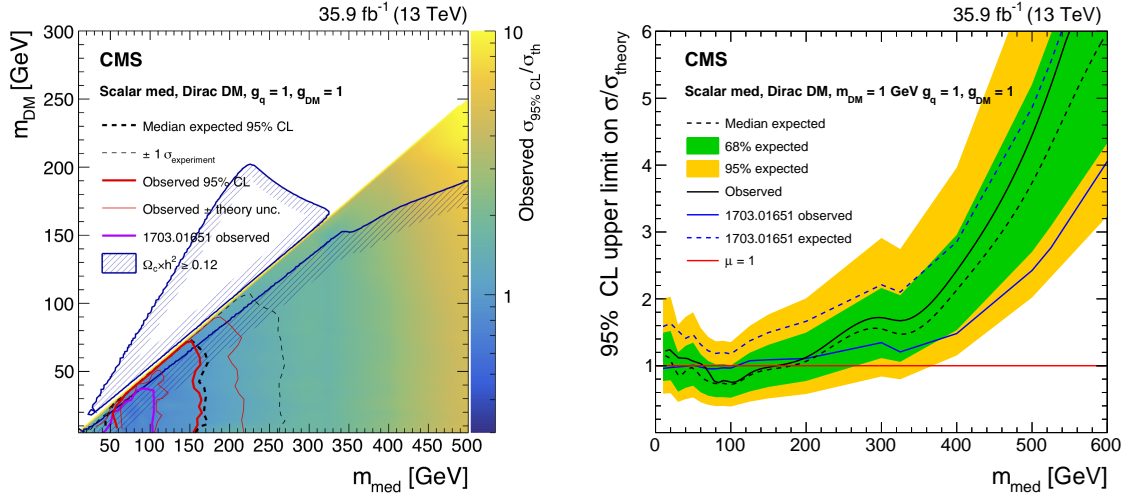


Figure 22: Exclusion limits at 95% CL on $\mu = \sigma/\sigma_{\text{th}}$ in the $m_{\text{med}}-m_{\text{DM}}$ plane assuming scalar mediators (left) allowing for vector boson couplings simulated at LO in QCD. The solid (dotted) red (black) line shows the contour for the observed (expected) exclusion. The solid contours around the observed limit and the dashed contours around the expected limit represent one standard deviation due to theoretical uncertainties in the signal cross section and the quadratic sum of the statistical and experimental systematic uncertainties, respectively. Expected and observed sensitivity of the previous CMS publication [14] are also presented. Results of the Planck satellite experiment [97] are shown as dark blue contours. In the shaded area DM is overabundant. Expected (dotted black line) and observed (solid black line) 95% CL upper limits on the signal strength μ as a function of the mediator mass for the spin-0 models (right).

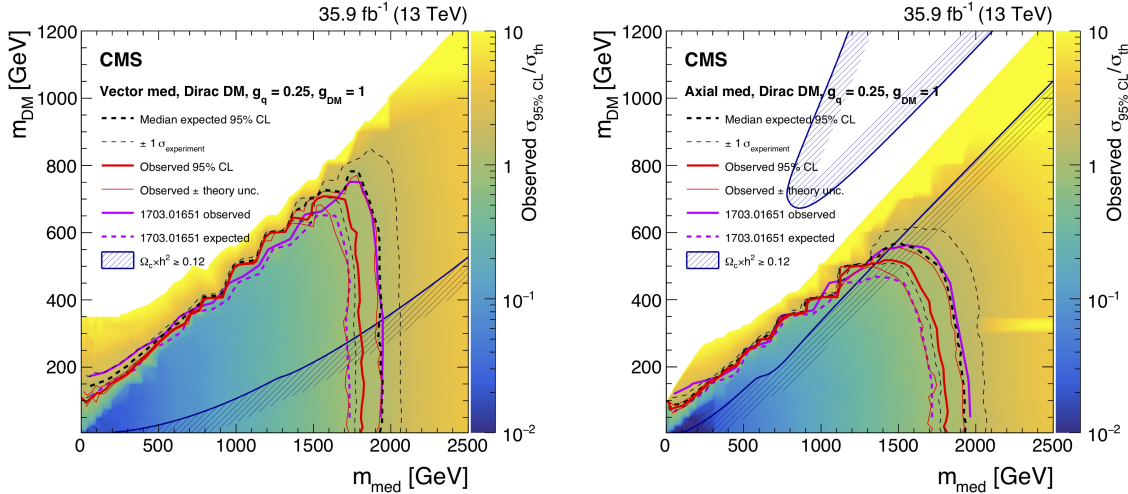


Figure 23: Exclusion limits at 95% CL on $\mu = \sigma/\sigma_{\text{th}}$ in the $m_{\text{med}}-m_{\text{DM}}$ plane assuming vector (left) and axial-vector (right) mediators where the the mono-V signal is simulated at LO in QCD. The solid (dotted) red (black) line shows the contour for the observed (expected) exclusion. The solid contours around the observed limit and the dashed contours around the expected limit represent one standard deviation due to theoretical uncertainties in the signal cross section and the quadratic sum of the statistical and experimental systematic uncertainties, respectively. Planck satellite experiment [97] are shown as dark blue contours. In the shaded area DM is overabundant.

B The CMS Collaboration

Yerevan Physics Institute, Yerevan, Armenia

A.M. Sirunyan, A. Tumasyan

Institut für Hochenergiephysik, Wien, Austria

W. Adam, F. Ambrogio, E. Asilar, T. Bergauer, J. Brandstetter, E. Brondolin, M. Dragicevic, J. Erö, A. Escalante Del Valle, M. Flechl, M. Friedl, R. Frühwirth¹, V.M. Ghete, J. Grossmann, J. Hrubec, M. Jeitler¹, A. König, N. Krammer, I. Krätschmer, D. Liko, T. Madlener, I. Mikulec, E. Pree, N. Rad, H. Rohringer, J. Schieck¹, R. Schöfbeck, M. Spanring, D. Spitzbart, A. Taurok, W. Waltenberger, J. Wittmann, C.-E. Wulz¹, M. Zarucki

Institute for Nuclear Problems, Minsk, Belarus

V. Chekhovsky, V. Mossolov, J. Suarez Gonzalez

Universiteit Antwerpen, Antwerpen, Belgium

E.A. De Wolf, D. Di Croce, X. Janssen, J. Lauwers, M. Van De Klundert, H. Van Haeuvermaet, P. Van Mechelen, N. Van Remortel

Vrije Universiteit Brussel, Brussel, Belgium

S. Abu Zeid, F. Blekman, J. D'Hondt, I. De Bruyn, J. De Clercq, K. Deroover, G. Flouris, D. Lontkovskyi, S. Lowette, I. Marchesini, S. Moortgat, L. Moreels, Q. Python, K. Skovpen, S. Tavernier, W. Van Doninck, P. Van Mulders, I. Van Parijs

Université Libre de Bruxelles, Bruxelles, Belgium

D. Beghin, B. Bilin, H. Brun, B. Clerboux, G. De Lentdecker, H. Delannoy, B. Dorney, G. Fasanella, L. Favart, R. Goldouzian, A. Grebenyuk, A.K. Kalsi, T. Lenzi, J. Luetic, T. Maerschalk, A. Marinov, T. Seva, E. Starling, C. Vander Velde, P. Vanlaer, D. Vannerom, R. Yonamine, F. Zenoni

Ghent University, Ghent, Belgium

T. Cornelis, D. Dobur, A. Fagot, M. Gul, I. Khvastunov², D. Poyraz, C. Roskas, S. Salva, M. Tytgat, W. Verbeke, N. Zaganidis

Université Catholique de Louvain, Louvain-la-Neuve, Belgium

H. Bakhshiansohi, O. Bondu, S. Brochet, G. Bruno, C. Caputo, A. Caudron, P. David, S. De Visscher, C. Delaere, M. Delcourt, B. Francois, A. Giammanco, M. Komm, G. Krintiras, V. Lemaître, A. Magitteri, A. Mertens, M. Musich, K. Piotrkowski, L. Quertenmont, A. Saggio, M. Vidal Marono, S. Wertz, J. Zobec

Centro Brasileiro de Pesquisas Físicas, Rio de Janeiro, Brazil

W.L. Aldá Júnior, F.L. Alves, G.A. Alves, L. Brito, M. Correa Martins Junior, G. Correia Silva, C. Hensel, A. Moraes, M.E. Pol, P. Rebello Teles

Universidade do Estado do Rio de Janeiro, Rio de Janeiro, Brazil

E. Belchior Batista Das Chagas, W. Carvalho, J. Chinellato³, E. Coelho, E.M. Da Costa, G.G. Da Silveira⁴, D. De Jesus Damiao, S. Fonseca De Souza, L.M. Huertas Guativa, H. Malbouisson, M. Melo De Almeida, C. Mora Herrera, L. Mundim, H. Nogima, L.J. Sanchez Rosas, A. Santoro, A. Sznajder, M. Thiel, E.J. Tonelli Manganote³, F. Torres Da Silva De Araujo, A. Vilela Pereira

Universidade Estadual Paulista ^a, Universidade Federal do ABC ^b, São Paulo, Brazil

S. Ahuja^a, C.A. Bernardes^a, T.R. Fernandez Perez Tomei^a, E.M. Gregores^b, P.G. Mercadante^b, S.F. Novaes^a, Sandra S. Padula^a, D. Romero Abad^b, J.C. Ruiz Vargas^a

Institute for Nuclear Research and Nuclear Energy, Bulgarian Academy of Sciences, Sofia, Bulgaria

A. Aleksandrov, R. Hadjiiska, P. Iaydjiev, M. Misheva, M. Rodozov, M. Shopova, G. Sultanov

University of Sofia, Sofia, Bulgaria

A. Dimitrov, L. Litov, B. Pavlov, P. Petkov

Beihang University, Beijing, China

W. Fang⁵, X. Gao⁵, L. Yuan

Institute of High Energy Physics, Beijing, China

M. Ahmad, J.G. Bian, G.M. Chen, H.S. Chen, M. Chen, Y. Chen, C.H. Jiang, D. Leggat, H. Liao, Z. Liu, F. Romeo, S.M. Shaheen, A. Spiezia, J. Tao, C. Wang, Z. Wang, E. Yazgan, T. Yu, H. Zhang, S. Zhang, J. Zhao

State Key Laboratory of Nuclear Physics and Technology, Peking University, Beijing, China

Y. Ban, G. Chen, J. Li, Q. Li, S. Liu, Y. Mao, S.J. Qian, D. Wang, Z. Xu, F. Zhang⁵

Tsinghua University, Beijing, China

Y. Wang

Universidad de Los Andes, Bogota, Colombia

C. Avila, A. Cabrera, C.A. Carrillo Montoya, L.F. Chaparro Sierra, C. Florez, C.F. González Hernández, J.D. Ruiz Alvarez, M.A. Segura Delgado

University of Split, Faculty of Electrical Engineering, Mechanical Engineering and Naval Architecture, Split, Croatia

B. Courbon, N. Godinovic, D. Lelas, I. Puljak, P.M. Ribeiro Cipriano, T. Sculac

University of Split, Faculty of Science, Split, Croatia

Z. Antunovic, M. Kovac

Institute Rudjer Boskovic, Zagreb, Croatia

V. Brigljevic, D. Ferencek, K. Kadija, B. Mesic, A. Starodumov⁶, T. Susa

University of Cyprus, Nicosia, Cyprus

M.W. Ather, A. Attikis, G. Mavromanolakis, J. Mousa, C. Nicolaou, F. Ptochos, P.A. Razis, H. Rykaczewski

Charles University, Prague, Czech Republic

M. Finger⁷, M. Finger Jr.⁷

Universidad San Francisco de Quito, Quito, Ecuador

E. Carrera Jarrin

Academy of Scientific Research and Technology of the Arab Republic of Egypt, Egyptian Network of High Energy Physics, Cairo, Egypt

Y. Assran^{8,9}, S. Elgammal⁹, S. Khalil¹⁰

National Institute of Chemical Physics and Biophysics, Tallinn, Estonia

S. Bhowmik, R.K. Dewanjee, M. Kadastik, L. Perrini, M. Raidal, A. Tiko, C. Veelken

Department of Physics, University of Helsinki, Helsinki, Finland

P. Eerola, H. Kirschenmann, J. Pekkanen, M. Voutilainen

Helsinki Institute of Physics, Helsinki, Finland

J. Havukainen, J.K. Heikkilä, T. Järvinen, V. Karimäki, R. Kinnunen, T. Lampén, K. Lassila-Perini, S. Laurila, S. Lehti, T. Lindén, P. Luukka, T. Mäenpää, H. Siikonen, E. Tuominen, J. Tuominiemi

Lappeenranta University of Technology, Lappeenranta, Finland

T. Tuuva

IRFU, CEA, Université Paris-Saclay, Gif-sur-Yvette, France

M. Besancon, F. Couderc, M. Dejardin, D. Denegri, J.L. Faure, F. Ferri, S. Ganjour, S. Ghosh, A. Givernaud, P. Gras, G. Hamel de Monchenault, P. Jarry, I. Kucher, C. Leloup, E. Locci, M. Machet, J. Malcles, G. Negro, J. Rander, A. Rosowsky, M.Ö. Sahin, M. Titov

Laboratoire Leprince-Ringuet, Ecole polytechnique, CNRS/IN2P3, Université Paris-Saclay, Palaiseau, France

A. Abdulsalam¹¹, C. Amendola, I. Antropov, S. Baffioni, F. Beaudette, P. Busson, L. Cadamuro, C. Charlot, R. Granier de Cassagnac, M. Jo, S. Lisniak, A. Lobanov, J. Martin Blanco, M. Nguyen, C. Ochando, G. Ortona, P. Paganini, P. Pigard, R. Salerno, J.B. Sauvan, Y. Sirois, A.G. Stahl Leitner, T. Strebler, Y. Yilmaz, A. Zabi, A. Zghiche

Université de Strasbourg, CNRS, IPHC UMR 7178, F-67000 Strasbourg, France

J.-L. Agram¹², J. Andrea, D. Bloch, J.-M. Brom, M. Buttignol, E.C. Chabert, N. Chanon, C. Collard, E. Conte¹², X. Coubez, F. Drouhin¹², J.-C. Fontaine¹², D. Gelé, U. Goerlach, M. Jansová, P. Juillot, A.-C. Le Bihan, N. Taroni, P. Van Hove

Centre de Calcul de l'Institut National de Physique Nucleaire et de Physique des Particules, CNRS/IN2P3, Villeurbanne, France

S. Gadrat

Université de Lyon, Université Claude Bernard Lyon 1, CNRS-IN2P3, Institut de Physique Nucléaire de Lyon, Villeurbanne, France

S. Beauceron, C. Bernet, G. Boudoul, R. Chierici, D. Contardo, P. Depasse, H. El Mamouni, J. Fay, L. Finco, S. Gascon, M. Gouzevitch, G. Grenier, B. Ille, F. Lagarde, I.B. Laktineh, M. Lethuillier, L. Mirabito, A.L. Pequegnot, S. Perries, A. Popov¹³, V. Sordini, M. Vander Donckt, S. Viret

Georgian Technical University, Tbilisi, Georgia

T. Toriashvili¹⁴

Tbilisi State University, Tbilisi, Georgia

Z. Tsamalaidze⁷

RWTH Aachen University, I. Physikalisches Institut, Aachen, Germany

C. Autermann, L. Feld, M.K. Kiesel, K. Klein, M. Lipinski, M. Preuten, C. Schomakers, J. Schulz, M. Teroerde, B. Wittmer, V. Zhukov¹³

RWTH Aachen University, III. Physikalisches Institut A, Aachen, Germany

A. Albert, D. Duchardt, M. Endres, M. Erdmann, S. Erdweg, T. Esch, R. Fischer, A. Güth, M. Hamer, T. Hebbeker, C. Heidemann, K. Hoepfner, S. Knutzen, M. Merschmeyer, A. Meyer, P. Millet, S. Mukherjee, T. Pook, M. Radziej, H. Reithler, M. Rieger, F. Scheuch, D. Teyssier, S. Thüer

RWTH Aachen University, III. Physikalisches Institut B, Aachen, Germany

G. Flügge, B. Kargoll, T. Kress, A. Künsken, T. Müller, A. Nehr Korn, A. Nowack, C. Pistone, O. Pooth, A. Stahl¹⁵

Deutsches Elektronen-Synchrotron, Hamburg, Germany

M. Aldaya Martin, T. Arndt, C. Asawatangtrakuldee, K. Beernaert, O. Behnke, U. Behrens, A. Bermúdez Martínez, A.A. Bin Anuar, K. Borras¹⁶, V. Botta, A. Campbell, P. Connor, C. Contreras-Campana, F. Costanza, C. Diez Pardos, G. Eckerlin, D. Eckstein, T. Eichhorn, E. Eren, E. Gallo¹⁷, J. Garay Garcia, A. Geiser, J.M. Grados Luyando, A. Grohsjean, P. Gunnellini, M. Guthoff, A. Harb, J. Hauk, M. Hempel¹⁸, H. Jung, M. Kasemann, J. Keaveney, C. Kleinwort, I. Korol, D. Krücker, W. Lange, A. Lelek, T. Lenz, J. Leonard, K. Lipka, W. Lohmann¹⁸, R. Mankel, I.-A. Melzer-Pellmann, A.B. Meyer, G. Mittag, J. Mnich, A. Mussgiller, E. Ntomari, D. Pitzl, A. Raspereza, M. Savitskyi, P. Saxena, R. Shevchenko, N. Stefaniuk, G.P. Van Onsem, R. Walsh, Y. Wen, K. Wichmann, C. Wissing, O. Zenaiev

University of Hamburg, Hamburg, Germany

R. Aggleton, S. Bein, V. Blobel, M. Centis Vignali, T. Dreyer, E. Garutti, D. Gonzalez, J. Haller, A. Hinzmann, M. Hoffmann, A. Karavdina, R. Klanner, R. Kogler, N. Kovalchuk, S. Kurz, T. Lapsien, D. Marconi, M. Meyer, M. Niedziela, D. Nowatschin, F. Pantaleo¹⁵, T. Peiffer, A. Perieanu, C. Scharf, P. Schleper, A. Schmidt, S. Schumann, J. Schwandt, J. Sonneveld, H. Stadie, G. Steinbrück, F.M. Stober, M. Stöver, H. Tholen, D. Troendle, E. Usai, A. Vanhoeyer, B. Vormwald

Institut für Experimentelle Kernphysik, Karlsruhe, Germany

M. Akbiyik, C. Barth, M. Baselga, S. Baur, E. Butz, R. Caspart, T. Chwalek, F. Colombo, W. De Boer, A. Dierlamm, N. Faltermann, B. Freund, R. Friese, M. Giffels, M.A. Harrendorf, F. Hartmann¹⁵, S.M. Heindl, U. Husemann, F. Kassel¹⁵, S. Kudella, H. Mildner, M.U. Mozer, Th. Müller, M. Plagge, G. Quast, K. Rabbertz, M. Schröder, I. Shvetsov, G. Sieber, H.J. Simonis, R. Ulrich, S. Wayand, M. Weber, T. Weiler, S. Williamson, C. Wöhrmann, R. Wolf

Institute of Nuclear and Particle Physics (INPP), NCSR Demokritos, Aghia Paraskevi, Greece

G. Anagnostou, G. Daskalakis, T. Gerasis, A. Kyriakis, D. Loukas, I. Topsis-Giotis

National and Kapodistrian University of Athens, Athens, Greece

G. Karathanasis, S. Kesisoglou, A. Panagiotou, N. Saoulidou

National Technical University of Athens, Athens, Greece

K. Kousouris

University of Ioánnina, Ioánnina, Greece

I. Evangelou, C. Foudas, P. Gianneios, P. Katsoulis, P. Kokkas, S. Mallios, N. Manthos, I. Papadopoulos, E. Paradas, J. Strologas, F.A. Triantis, D. Tsitsonis

MTA-ELTE Lendület CMS Particle and Nuclear Physics Group, Eötvös Loránd University, Budapest, Hungary

M. Csanad, N. Filipovic, G. Pasztor, O. Surányi, G.I. Veres¹⁹

Wigner Research Centre for Physics, Budapest, Hungary

G. Bencze, C. Hajdu, D. Horvath²⁰, Á. Hunyadi, F. Sikler, V. Veszpremi, G. Vesztergombi¹⁹

Institute of Nuclear Research ATOMKI, Debrecen, Hungary

N. Beni, S. Czellar, J. Karancsi²¹, A. Makovec, J. Molnar, Z. Szillasi

Institute of Physics, University of Debrecen, Debrecen, Hungary

M. Bartók¹⁹, P. Raics, Z.L. Trocsanyi, B. Ujvari

Indian Institute of Science (IISc), Bangalore, India

S. Choudhury, J.R. Komaragiri

National Institute of Science Education and Research, Bhubaneswar, India

S. Bahinipati²², P. Mal, K. Mandal, A. Nayak²³, D.K. Sahoo²², N. Sahoo, S.K. Swain

Panjab University, Chandigarh, India

S. Bansal, S.B. Beri, V. Bhatnagar, R. Chawla, N. Dhingra, A. Kaur, M. Kaur, S. Kaur, R. Kumar, P. Kumari, A. Mehta, J.B. Singh, G. Walia

University of Delhi, Delhi, India

Ashok Kumar, Aashaq Shah, A. Bhardwaj, S. Chauhan, B.C. Choudhary, R.B. Garg, S. Keshri, A. Kumar, S. Malhotra, M. Naimuddin, K. Ranjan, R. Sharma

Saha Institute of Nuclear Physics, HBNI, Kolkata, India

R. Bhardwaj, R. Bhattacharya, S. Bhattacharya, U. Bhawandeep, S. Dey, S. Dutt, S. Dutta, S. Ghosh, N. Majumdar, A. Modak, K. Mondal, S. Mukhopadhyay, S. Nandan, A. Purohit, A. Roy, S. Roy Chowdhury, S. Sarkar, M. Sharan, S. Thakur

Indian Institute of Technology Madras, Madras, India

P.K. Behera

Bhabha Atomic Research Centre, Mumbai, India

R. Chudasama, D. Dutta, V. Jha, V. Kumar, A.K. Mohanty¹⁵, P.K. Netrakanti, L.M. Pant, P. Shukla, A. Topkar

Tata Institute of Fundamental Research-A, Mumbai, India

T. Aziz, S. Dugad, B. Mahakud, S. Mitra, G.B. Mohanty, N. Sur, B. Sutar

Tata Institute of Fundamental Research-B, Mumbai, India

S. Banerjee, S. Bhattacharya, S. Chatterjee, P. Das, M. Guchait, Sa. Jain, S. Kumar, M. Maity²⁴, G. Majumder, K. Mazumdar, T. Sarkar²⁴, N. Wickramage²⁵

Indian Institute of Science Education and Research (IISER), Pune, India

S. Chauhan, S. Dube, V. Hegde, A. Kapoor, K. Kothekar, S. Pandey, A. Rane, S. Sharma

Institute for Research in Fundamental Sciences (IPM), Tehran, Iran

S. Chenarani²⁶, E. Eskandari Tadavani, S.M. Etesami²⁶, M. Khakzad, M. Mohammadi Najafabadi, M. Naseri, S. Paktinat Mehdiabadi²⁷, F. Rezaei Hosseinabadi, B. Safarzadeh²⁸, M. Zeinali

University College Dublin, Dublin, Ireland

M. Felcini, M. Grunewald

INFN Sezione di Bari ^a, Università di Bari ^b, Politecnico di Bari ^c, Bari, Italy

M. Abbrescia^{a,b}, C. Calabria^{a,b}, A. Colaleo^a, D. Creanza^{a,c}, L. Cristella^{a,b}, N. De Filippis^{a,c}, M. De Palma^{a,b}, F. Errico^{a,b}, L. Fiore^a, G. Iaselli^{a,c}, S. Lezki^{a,b}, G. Maggi^{a,c}, M. Maggi^a, G. Miniello^{a,b}, S. My^{a,b}, S. Nuzzo^{a,b}, A. Pompili^{a,b}, G. Pugliese^{a,c}, R. Radogna^a, A. Ranieri^a, G. Selvaggi^{a,b}, A. Sharma^a, L. Silvestris^{a,15}, R. Venditti^a, P. Verwilligen^a

INFN Sezione di Bologna ^a, Università di Bologna ^b, Bologna, Italy

G. Abbiendi^a, C. Battilana^{a,b}, D. Bonacorsi^{a,b}, L. Borgonovi^{a,b}, S. Braibant-Giacomelli^{a,b}, R. Campanini^{a,b}, P. Capiluppi^{a,b}, A. Castro^{a,b}, F.R. Cavallo^a, S.S. Chhibra^{a,b}, G. Codispoti^{a,b}, M. Cuffiani^{a,b}, G.M. Dallavalle^a, F. Fabbri^a, A. Fanfani^{a,b}, D. Fasanella^{a,b}, P. Giacomelli^a, C. Grandi^a, L. Guiducci^{a,b}, S. Marcellini^a, G. Masetti^a, A. Montanari^a, F.L. Navarria^{a,b}, A. Perrotta^a, A.M. Rossi^{a,b}, T. Rovelli^{a,b}, G.P. Siroli^{a,b}, N. Tosi^a

INFN Sezione di Catania ^a, Università di Catania ^b, Catania, Italy

S. Albergo^{a,b}, S. Costa^{a,b}, A. Di Mattia^a, F. Giordano^{a,b}, R. Potenza^{a,b}, A. Tricomi^{a,b}, C. Tuve^{a,b}

INFN Sezione di Firenze ^a, Università di Firenze ^b, Firenze, Italy

G. Barbagli^a, K. Chatterjee^{a,b}, V. Ciulli^{a,b}, C. Civinini^a, R. D'Alessandro^{a,b}, E. Focardi^{a,b}, P. Lenzi^{a,b}, M. Meschini^a, S. Paoletti^a, L. Russo^{a,29}, G. Sguazzoni^a, D. Strom^a, L. Viliani^a

INFN Laboratori Nazionali di Frascati, Frascati, Italy

L. Benussi, S. Bianco, F. Fabbri, D. Piccolo, F. Primavera¹⁵

INFN Sezione di Genova ^a, Università di Genova ^b, Genova, Italy

V. Calvelli^{a,b}, F. Ferro^a, F. Ravera^{a,b}, E. Robutti^a, S. Tosi^{a,b}

INFN Sezione di Milano-Bicocca ^a, Università di Milano-Bicocca ^b, Milano, Italy

A. Benaglia^a, A. Beschi^b, L. Brianza^{a,b}, F. Brivio^{a,b}, V. Ciriolo^{a,b,15}, M.E. Dinardo^{a,b}, S. Fiorendi^{a,b}, S. Gennai^a, A. Ghezzi^{a,b}, P. Govoni^{a,b}, M. Malberti^{a,b}, S. Malvezzi^a, R.A. Manzoni^{a,b}, D. Menasce^a, L. Moroni^a, M. Paganoni^{a,b}, K. Pauwels^{a,b}, D. Pedrini^a, S. Pigazzini^{a,b,30}, S. Ragazzi^{a,b}, T. Tabarelli de Fatis^{a,b}

INFN Sezione di Napoli ^a, Università di Napoli 'Federico II' ^b, Napoli, Italy, Università della Basilicata ^c, Potenza, Italy, Università G. Marconi ^d, Roma, Italy

S. Buontempo^a, N. Cavallo^{a,c}, S. Di Guida^{a,d,15}, F. Fabozzi^{a,c}, F. Fienga^{a,b}, A.O.M. Iorio^{a,b}, W.A. Khan^a, L. Lista^a, S. Meola^{a,d,15}, P. Paolucci^{a,15}, C. Sciacca^{a,b}, F. Thyssen^a

INFN Sezione di Padova ^a, Università di Padova ^b, Padova, Italy, Università di Trento ^c, Trento, Italy

P. Azzi^a, N. Bacchetta^a, L. Benato^{a,b}, D. Bisello^{a,b}, A. Boletti^{a,b}, R. Carlin^{a,b}, P. Checchia^a, M. Dall'Osso^{a,b}, P. De Castro Manzano^a, T. Dorigo^a, U. Dosselli^a, F. Gasparini^{a,b}, U. Gasparini^{a,b}, A. Gozzelino^a, S. Lacaprara^a, P. Lujan, M. Margoni^{a,b}, A.T. Meneguzzo^{a,b}, N. Pozzobon^{a,b}, P. Ronchese^{a,b}, R. Rossin^{a,b}, E. Torassa^a, S. Ventura^a, M. Zanetti^{a,b}, P. Zotto^{a,b}, G. Zumerle^{a,b}

INFN Sezione di Pavia ^a, Università di Pavia ^b, Pavia, Italy

A. Braghieri^a, A. Magnani^a, P. Montagna^{a,b}, S.P. Ratti^{a,b}, V. Re^a, M. Ressegotti^{a,b}, C. Riccardi^{a,b}, P. Salvini^a, I. Vai^{a,b}, P. Vitulo^{a,b}

INFN Sezione di Perugia ^a, Università di Perugia ^b, Perugia, Italy

L. Alunni Solestizi^{a,b}, M. Biasini^{a,b}, G.M. Bilei^a, C. Cecchi^{a,b}, D. Ciangottini^{a,b}, L. Fanò^{a,b}, P. Lariccia^{a,b}, R. Leonardi^{a,b}, E. Manoni^a, G. Mantovani^{a,b}, V. Mariani^{a,b}, M. Menichelli^a, A. Rossi^{a,b}, A. Santocchia^{a,b}, D. Spiga^a

INFN Sezione di Pisa ^a, Università di Pisa ^b, Scuola Normale Superiore di Pisa ^c, Pisa, Italy

K. Androsov^a, P. Azzurri^{a,15}, G. Bagliesi^a, T. Boccali^a, L. Borrello, R. Castaldi^a, M.A. Ciocci^{a,b}, R. Dell'Orso^a, G. Fedì^a, L. Giannini^{a,c}, A. Giassi^a, M.T. Grippo^{a,29}, F. Ligabue^{a,c}, T. Lomtadze^a, E. Manca^{a,c}, G. Mandorli^{a,c}, A. Messineo^{a,b}, F. Palla^a, A. Rizzi^{a,b}, A. Savoy-Navarro^{a,31}, P. Spagnolo^a, R. Tenchini^a, G. Tonelli^{a,b}, A. Venturi^a, P.G. Verdini^a

INFN Sezione di Roma ^a, Sapienza Università di Roma ^b, Rome, Italy

L. Barone^{a,b}, F. Cavallari^a, M. Cipriani^{a,b}, N. Daci^a, D. Del Re^{a,b,15}, E. Di Marco^{a,b}, M. Diemoz^a, S. Gelli^{a,b}, E. Longo^{a,b}, F. Margaroli^{a,b}, B. Marzocchi^{a,b}, P. Meridiani^a, G. Organtini^{a,b}, R. Paramatti^{a,b}, F. Preiato^{a,b}, S. Rahatlou^{a,b}, C. Rovelli^a, F. Santanastasio^{a,b}

INFN Sezione di Torino ^a, Università di Torino ^b, Torino, Italy, Università del Piemonte Orientale ^c, Novara, Italy

N. Amapane^{a,b}, R. Arcidiacono^{a,c}, S. Argiro^{a,b}, M. Arneodo^{a,c}, N. Bartosik^a, R. Bellan^{a,b}, C. Biino^a, N. Cartiglia^a, F. Cenna^{a,b}, M. Costa^{a,b}, R. Covarelli^{a,b}, A. Degano^{a,b}, N. Demaria^a, B. Kiani^{a,b}, C. Mariotti^a, S. Maselli^a, E. Migliore^{a,b}, V. Monaco^{a,b}, E. Monteil^{a,b}, M. Monteno^a

M.M. Obertino^{a,b}, L. Pacher^{a,b}, N. Pastrone^a, M. Pelliccioni^a, G.L. Pinna Angioni^{a,b}, A. Romero^{a,b}, M. Ruspa^{a,c}, R. Sacchi^{a,b}, K. Shchelina^{a,b}, V. Sola^a, A. Solano^{a,b}, A. Staiano^a, P. Traczyk^{a,b}

INFN Sezione di Trieste ^a, Università di Trieste ^b, Trieste, Italy

S. Belforte^a, M. Casarsa^a, F. Cossutti^a, G. Della Ricca^{a,b}, A. Zanetti^a

Kyungpook National University, Daegu, Korea

D.H. Kim, G.N. Kim, M.S. Kim, J. Lee, S. Lee, S.W. Lee, C.S. Moon, Y.D. Oh, S. Sekmen, D.C. Son, Y.C. Yang

Chonbuk National University, Jeonju, Korea

A. Lee

Chonnam National University, Institute for Universe and Elementary Particles, Kwangju, Korea

H. Kim, D.H. Moon, G. Oh

Hanyang University, Seoul, Korea

J.A. Brochero Cifuentes, J. Goh, T.J. Kim

Korea University, Seoul, Korea

S. Cho, S. Choi, Y. Go, D. Gyun, S. Ha, B. Hong, Y. Jo, Y. Kim, K. Lee, K.S. Lee, S. Lee, J. Lim, S.K. Park, Y. Roh

Seoul National University, Seoul, Korea

J. Almond, J. Kim, J.S. Kim, H. Lee, K. Lee, K. Nam, S.B. Oh, B.C. Radburn-Smith, S.h. Seo, U.K. Yang, H.D. Yoo, G.B. Yu

University of Seoul, Seoul, Korea

H. Kim, J.H. Kim, J.S.H. Lee, I.C. Park

Sungkyunkwan University, Suwon, Korea

Y. Choi, C. Hwang, J. Lee, I. Yu

Vilnius University, Vilnius, Lithuania

V. Dudenas, A. Juodagalvis, J. Vaitkus

National Centre for Particle Physics, Universiti Malaya, Kuala Lumpur, Malaysia

I. Ahmed, Z.A. Ibrahim, M.A.B. Md Ali³², F. Mohamad Idris³³, W.A.T. Wan Abdullah, M.N. Yusli, Z. Zolkapli

Centro de Investigacion y de Estudios Avanzados del IPN, Mexico City, Mexico

Reyes-Almanza, R, Ramirez-Sanchez, G., Duran-Osuna, M. C., H. Castilla-Valdez, E. De La Cruz-Burelo, I. Heredia-De La Cruz³⁴, Rabadan-Trejo, R. I., R. Lopez-Fernandez, J. Mejia Guisao, A. Sanchez-Hernandez

Universidad Iberoamericana, Mexico City, Mexico

S. Carrillo Moreno, C. Oropeza Barrera, F. Vazquez Valencia

Benemerita Universidad Autonoma de Puebla, Puebla, Mexico

J. Eysermans, I. Pedraza, H.A. Salazar Ibarquen, C. Uribe Estrada

Universidad Autónoma de San Luis Potosí, San Luis Potosí, Mexico

A. Morelos Pineda

University of Auckland, Auckland, New Zealand

D. Krofcheck

University of Canterbury, Christchurch, New Zealand

P.H. Butler

National Centre for Physics, Quaid-I-Azam University, Islamabad, Pakistan

A. Ahmad, M. Ahmad, Q. Hassan, H.R. Hoorani, A. Saddique, M.A. Shah, M. Shoaib, M. Waqas

National Centre for Nuclear Research, Swierk, Poland

H. Bialkowska, M. Bluj, B. Boimska, T. Frueboes, M. Górski, M. Kazana, K. Nawrocki, M. Szleper, P. Zalewski

Institute of Experimental Physics, Faculty of Physics, University of Warsaw, Warsaw, PolandK. Bunkowski, A. Byszuk³⁵, K. Doroba, A. Kalinowski, M. Konecki, J. Krolikowski, M. Misiura, M. Olszewski, A. Pyskir, M. Walczak**Laboratório de Instrumentação e Física Experimental de Partículas, Lisboa, Portugal**

P. Bargassa, C. Beirão Da Cruz E Silva, A. Di Francesco, P. Faccioli, B. Galinhas, M. Gallinaro, J. Hollar, N. Leonardo, L. Lloret Iglesias, M.V. Nemallapudi, J. Seixas, G. Strong, O. Toldaiev, D. Vadrucio, J. Varela

Joint Institute for Nuclear Research, Dubna, RussiaS. Afanasiev, V. Alexakhin, M. Gavrilenko, A. Golunov, I. Golutvin, N. Gorbounov, V. Karjavin, A. Lanev, A. Malakhov, V. Matveev^{36,37}, P. Moiseenz, V. Palichik, V. Perelygin, M. Savina, S. Shmatov, N. Skatchkov, V. Smirnov, N. Voytishin, A. Zarubin**Petersburg Nuclear Physics Institute, Gatchina (St. Petersburg), Russia**Y. Ivanov, V. Kim³⁸, E. Kuznetsova³⁹, P. Levchenko, V. Murzin, V. Oreshkin, I. Smirnov, D. Sosnov, V. Sulimov, L. Uvarov, S. Vavilov, A. Vorobyev**Institute for Nuclear Research, Moscow, Russia**

Yu. Andreev, A. Dermenev, S. Gninenko, N. Golubev, A. Karneyeu, M. Kirsanov, N. Krasnikov, A. Pashenkov, D. Tlisov, A. Toropin

Institute for Theoretical and Experimental Physics, Moscow, Russia

V. Epshteyn, V. Gavrilov, N. Lychkovskaya, V. Popov, I. Pozdnyakov, G. Safronov, A. Spiridonov, A. Stepenov, V. Stolin, M. Toms, E. Vlasov, A. Zhokin

Moscow Institute of Physics and Technology, Moscow, RussiaT. Aushev, A. Bylinkin³⁷**National Research Nuclear University 'Moscow Engineering Physics Institute' (MEPhI), Moscow, Russia**M. Chadeeva⁴⁰, P. Parygin, D. Philippov, S. Polikarpov, E. Popova, V. Rusinov**P.N. Lebedev Physical Institute, Moscow, Russia**V. Andreev, M. Azarkin³⁷, I. Dremin³⁷, M. Kirakosyan³⁷, S.V. Rusakov, A. Terkulov**Skobeltsyn Institute of Nuclear Physics, Lomonosov Moscow State University, Moscow, Russia**A. Baskakov, A. Belyaev, E. Boos, M. Dubinin⁴¹, L. Dudko, A. Ershov, A. Gribushin, V. Klyukhin, O. Kodolova, I. Lokhtin, I. Miagkov, S. Obraztsov, S. Petrushanko, V. Savrin, A. Snigirev

Novosibirsk State University (NSU), Novosibirsk, RussiaV. Blinov⁴², D. Shtol⁴², Y. Skovpen⁴²**State Research Center of Russian Federation, Institute for High Energy Physics of NRC "Kurchatov Institute", Protvino, Russia**

I. Azhgirey, I. Bayshev, S. Bitioukov, D. Elumakhov, A. Godizov, V. Kachanov, A. Kalinin, D. Konstantinov, P. Mandrik, V. Petrov, R. Ryutin, A. Sobol, S. Troshin, N. Tyurin, A. Uzunian, A. Volkov

University of Belgrade, Faculty of Physics and Vinca Institute of Nuclear Sciences, Belgrade, SerbiaP. Adzic⁴³, P. Cirkovic, D. Devetak, M. Dordevic, J. Milosevic, V. Rekovic**Centro de Investigaciones Energéticas Medioambientales y Tecnológicas (CIEMAT), Madrid, Spain**

J. Alcaraz Maestre, I. Bachiller, M. Barrio Luna, M. Cerrada, N. Colino, B. De La Cruz, A. Delgado Peris, C. Fernandez Bedoya, J.P. Fernández Ramos, J. Flix, M.C. Fouz, O. Gonzalez Lopez, S. Goy Lopez, J.M. Hernandez, M.I. Josa, D. Moran, A. Pérez-Calero Yzquierdo, J. Puerta Pelayo, I. Redondo, L. Romero, M.S. Soares, A. Álvarez Fernández

Universidad Autónoma de Madrid, Madrid, Spain

C. Albajar, J.F. de Trocóniz, M. Missiroli

Universidad de Oviedo, Oviedo, Spain

J. Cuevas, C. Erice, J. Fernandez Menendez, I. Gonzalez Caballero, J.R. González Fernández, E. Palencia Cortezon, S. Sanchez Cruz, P. Vischia, J.M. Vizan Garcia

Instituto de Física de Cantabria (IFCA), CSIC-Universidad de Cantabria, Santander, Spain

I.J. Cabrillo, A. Calderon, B. Chazin Quero, E. Curras, J. Duarte Campderros, M. Fernandez, J. Garcia-Ferrero, G. Gomez, A. Lopez Virto, J. Marco, C. Martinez Rivero, P. Martinez Ruiz del Arbol, F. Matorras, J. Piedra Gomez, T. Rodrigo, A. Ruiz-Jimeno, L. Scodellaro, N. Trevisani, I. Vila, R. Vilar Cortabitarte

CERN, European Organization for Nuclear Research, Geneva, SwitzerlandD. Abbaneo, B. Akgun, E. Auffray, P. Baillon, A.H. Ball, D. Barney, J. Bendavid, M. Bianco, P. Bloch, A. Bocci, C. Botta, T. Camporesi, R. Castello, M. Cepeda, G. Cerminara, E. Chapon, Y. Chen, D. d'Enterria, A. Dabrowski, V. Daponte, A. David, M. De Gruttola, A. De Roeck, N. Deelen, M. Dobson, T. du Pree, M. Dünser, N. Dupont, A. Elliott-Peisert, P. Everaerts, F. Fallavollita, G. Franzoni, J. Fulcher, W. Funk, D. Gigi, A. Gilbert, K. Gill, F. Glege, D. Gulhan, P. Harris, J. Hegeman, V. Innocente, A. Jafari, P. Janot, O. Karacheban¹⁸, J. Kieseler, V. Knünz, A. Kornmayer, M.J. Kortelainen, M. Krammer¹, C. Lange, P. Lecoq, C. Lourenço, M.T. Lucchini, L. Malgeri, M. Mannelli, A. Martelli, F. Meijers, J.A. Merlin, S. Mersi, E. Meschi, P. Milenovic⁴⁴, F. Moortgat, M. Mulders, H. Neugebauer, J. Ngadiuba, S. Orfanelli, L. Orsini, L. Pape, E. Perez, M. Peruzzi, A. Petrilli, G. Petrucciani, A. Pfeiffer, M. Pierini, D. Rabadý, A. Racz, T. Reis, G. Rolandi⁴⁵, M. Rovere, H. Sakulin, C. Schäfer, C. Schwick, M. Seidel, M. Selvaggi, A. Sharma, P. Silva, P. Sphicas⁴⁶, A. Stakia, J. Steggemann, M. Stoye, M. Tosi, D. Treille, A. Triossi, A. Tsirou, V. Veckalns⁴⁷, M. Verweij, W.D. Zeuner**Paul Scherrer Institut, Villigen, Switzerland**W. Bertl[†], L. Caminada⁴⁸, K. Deiters, W. Erdmann, R. Horisberger, Q. Ingram, H.C. Kaestli, D. Kotlinski, U. Langenegger, T. Rohe, S.A. Wiederkehr**ETH Zurich - Institute for Particle Physics and Astrophysics (IPA), Zurich, Switzerland**

M. Backhaus, L. Bäni, P. Berger, L. Bianchini, B. Casal, G. Dissertori, M. Dittmar, M. Donegà,

C. Dorfer, C. Grab, C. Heidegger, D. Hits, J. Hoss, G. Kasieczka, T. Klijsma, W. Lustermann, B. Mangano, M. Marionneau, M.T. Meinhard, D. Meister, F. Micheli, P. Musella, F. Nessi-Tedaldi, F. Pandolfi, J. Pata, F. Pauss, G. Perrin, L. Perrozzi, M. Quittnat, M. Reichmann, D.A. Sanz Becerra, M. Schönenberger, L. Shchutska, V.R. Tavolaro, K. Theofilatos, M.L. Vesterbacka Olsson, R. Wallny, D.H. Zhu

Universität Zürich, Zurich, Switzerland

T.K. Aarrestad, C. AMSler⁴⁹, M.F. Canelli, A. De Cosa, R. Del Burgo, S. Donato, C. Galloni, T. Hreus, B. Kilminster, D. Pinna, G. Rauco, P. Robmann, D. Salerno, K. Schweiger, C. Seitz, Y. Takahashi, A. Zucchetta

National Central University, Chung-Li, Taiwan

V. Candelise, Y.H. Chang, K.y. Cheng, T.H. Doan, Sh. Jain, R. Khurana, C.M. Kuo, W. Lin, A. Pozdnyakov, S.S. Yu

National Taiwan University (NTU), Taipei, Taiwan

Arun Kumar, P. Chang, Y. Chao, K.F. Chen, P.H. Chen, F. Fiori, W.-S. Hou, Y. Hsiung, Y.F. Liu, R.-S. Lu, E. Paganis, A. Psallidas, A. Steen, J.f. Tsai

Chulalongkorn University, Faculty of Science, Department of Physics, Bangkok, Thailand

B. Asavapibhop, K. Kovitangoon, G. Singh, N. Srimanobhas

Çukurova University, Physics Department, Science and Art Faculty, Adana, Turkey

A. Bat, F. Boran, S. Cerci⁵⁰, S. Damarseckin, Z.S. Demiroglu, C. Dozen, I. Dumanoglu, S. Girgis, G. Gokbulut, Y. Guler, I. Hos⁵¹, E.E. Kangal⁵², O. Kara, A. Kayis Topaksu, U. Kiminsu, M. Oglakci, G. Onengut⁵³, K. Ozdemir⁵⁴, D. Sunar Cerci⁵⁰, B. Tali⁵⁰, U.G. Tok, S. Turkcapar, I.S. Zorbakir, C. Zorbilmez

Middle East Technical University, Physics Department, Ankara, Turkey

G. Karapinar⁵⁵, K. Ocalan⁵⁶, M. Yalvac, M. Zeyrek

Bogazici University, Istanbul, Turkey

E. Gülmez, M. Kaya⁵⁷, O. Kaya⁵⁸, S. Tekten, E.A. Yetkin⁵⁹

Istanbul Technical University, Istanbul, Turkey

M.N. Agaras, S. Atay, A. Cakir, K. Cankocak, Y. Komurcu

Institute for Scintillation Materials of National Academy of Science of Ukraine, Kharkov, Ukraine

B. Grynyov

National Scientific Center, Kharkov Institute of Physics and Technology, Kharkov, Ukraine

L. Levchuk

University of Bristol, Bristol, United Kingdom

F. Ball, L. Beck, J.J. Brooke, D. Burns, E. Clement, D. Cussans, O. Davignon, H. Flacher, J. Goldstein, G.P. Heath, H.F. Heath, L. Kreczko, D.M. Newbold⁶⁰, S. Paramesvaran, T. Sakuma, S. Seif El Nasr-storey, D. Smith, V.J. Smith

Rutherford Appleton Laboratory, Didcot, United Kingdom

K.W. Bell, A. Belyaev⁶¹, C. Brew, R.M. Brown, L. Calligaris, D. Cieri, D.J.A. Cockerill, J.A. Coughlan, K. Harder, S. Harper, J. Linacre, E. Olaiya, D. Petyt, C.H. Shepherd-Themistocleous, A. Thea, I.R. Tomalin, T. Williams, W.J. Womersley

Imperial College, London, United Kingdom

G. Auzinger, R. Bainbridge, J. Borg, S. Breeze, O. Buchmuller, A. Bundock, S. Casasso,

M. Citron, D. Colling, L. Corpe, P. Dauncey, G. Davies, A. De Wit, M. Della Negra, R. Di Maria, A. Elwood, Y. Haddad, G. Hall, G. Iles, T. James, R. Lane, C. Laner, L. Lyons, A.-M. Magnan, S. Malik, L. Mastrolorenzo, T. Matsushita, J. Nash, A. Nikitenko⁶, V. Palladino, M. Pesaresi, D.M. Raymond, A. Richards, A. Rose, E. Scott, C. Seez, A. Shtipliyski, S. Summers, A. Tapper, K. Uchida, M. Vazquez Acosta⁶², T. Virdee¹⁵, N. Wardle, D. Winterbottom, J. Wright, S.C. Zenz

Brunel University, Uxbridge, United Kingdom

J.E. Cole, P.R. Hobson, A. Khan, P. Kyberd, I.D. Reid, L. Teodorescu, S. Zahid

Baylor University, Waco, USA

A. Borzou, K. Call, J. Dittmann, K. Hatakeyama, H. Liu, N. Pastika, C. Smith

Catholic University of America, Washington DC, USA

R. Bartek, A. Dominguez

The University of Alabama, Tuscaloosa, USA

A. Buccilli, S.I. Cooper, C. Henderson, P. Rumerio, C. West

Boston University, Boston, USA

D. Arcaro, A. Avetisyan, T. Bose, D. Gastler, D. Rankin, C. Richardson, J. Rohlf, L. Sulak, D. Zou

Brown University, Providence, USA

G. Benelli, D. Cutts, M. Hadley, J. Hakala, U. Heintz, J.M. Hogan, K.H.M. Kwok, E. Laird, G. Landsberg, J. Lee, Z. Mao, M. Narain, J. Pazzini, S. Piperov, S. Sagir, R. Syarif, D. Yu

University of California, Davis, Davis, USA

R. Band, C. Brainerd, R. Breedon, D. Burns, M. Calderon De La Barca Sanchez, M. Chertok, J. Conway, R. Conway, P.T. Cox, R. Erbacher, C. Flores, G. Funk, W. Ko, R. Lander, C. Mclean, M. Mulhearn, D. Pellett, J. Pilot, S. Shalhout, M. Shi, J. Smith, D. Stolp, K. Tos, M. Tripathi, Z. Wang

University of California, Los Angeles, USA

M. Bachtis, C. Bravo, R. Cousins, A. Dasgupta, A. Florent, J. Hauser, M. Ignatenko, N. Mccoll, S. Regnard, D. Saltzberg, C. Schnaible, V. Valuev

University of California, Riverside, Riverside, USA

E. Bouvier, K. Burt, R. Clare, J. Ellison, J.W. Gary, S.M.A. Ghiasi Shirazi, G. Hanson, J. Heilman, G. Karapostoli, E. Kennedy, F. Lacroix, O.R. Long, M. Olmedo Negrete, M.I. Paneva, W. Si, L. Wang, H. Wei, S. Wimpenny, B. R. Yates

University of California, San Diego, La Jolla, USA

J.G. Branson, S. Cittolin, M. Derdzinski, R. Gerosa, D. Gilbert, B. Hashemi, A. Holzner, D. Klein, G. Kole, V. Krutelyov, J. Letts, M. Masciovecchio, D. Olivito, S. Padhi, M. Pieri, M. Sani, V. Sharma, S. Simon, M. Tadel, A. Vartak, S. Wasserbaech⁶³, J. Wood, F. Würthwein, A. Yagil, G. Zevi Della Porta

University of California, Santa Barbara - Department of Physics, Santa Barbara, USA

N. Amin, R. Bhandari, J. Bradmiller-Feld, C. Campagnari, A. Dishaw, V. Dutta, M. Franco Sevilla, L. Gouskos, R. Heller, J. Incandela, A. Ovcharova, H. Qu, J. Richman, D. Stuart, I. Suarez, J. Yoo

California Institute of Technology, Pasadena, USA

D. Anderson, A. Bornheim, J. Bunn, J.M. Lawhorn, H.B. Newman, T. Q. Nguyen, C. Pena, M. Spiropulu, J.R. Vlimant, R. Wilkinson, S. Xie, Z. Zhang, R.Y. Zhu

Carnegie Mellon University, Pittsburgh, USA

M.B. Andrews, T. Ferguson, T. Mudholkar, M. Paulini, J. Russ, M. Sun, H. Vogel, I. Vorobiev, M. Weinberg

University of Colorado Boulder, Boulder, USA

J.P. Cumalat, W.T. Ford, F. Jensen, A. Johnson, M. Krohn, S. Leontsinis, T. Mulholland, K. Stenson, S.R. Wagner

Cornell University, Ithaca, USA

J. Alexander, J. Chaves, J. Chu, S. Dittmer, K. Mcdermott, N. Mirman, J.R. Patterson, D. Quach, A. Rinkevicius, A. Ryd, L. Skinnari, L. Soffi, S.M. Tan, Z. Tao, J. Thom, J. Tucker, P. Wittich, M. Zientek

Fermi National Accelerator Laboratory, Batavia, USA

S. Abdullin, M. Albrow, M. Alyari, G. Apollinari, A. Apresyan, A. Apyan, S. Banerjee, L.A.T. Bauerdick, A. Beretvas, J. Berryhill, P.C. Bhat, G. Bolla[†], K. Burkett, J.N. Butler, A. Canepa, G.B. Cerati, H.W.K. Cheung, F. Chlebana, M. Cremonesi, J. Duarte, V.D. Elvira, J. Freeman, Z. Gecse, E. Gottschalk, L. Gray, D. Green, S. Grünendahl, O. Gutsche, J. Hanlon, R.M. Harris, S. Hasegawa, J. Hirschauer, Z. Hu, B. Jayatilaka, S. Jindariani, M. Johnson, U. Joshi, B. Klima, B. Kreis, S. Lammel, D. Lincoln, R. Lipton, M. Liu, T. Liu, R. Lopes De Sá, J. Lykken, K. Maeshima, N. Magini, J.M. Marraffino, D. Mason, P. McBride, P. Merkel, S. Mrenna, S. Nahn, V. O'Dell, K. Pedro, O. Prokofyev, G. Rakness, L. Ristori, B. Schneider, E. Sexton-Kennedy, A. Soha, W.J. Spalding, L. Spiegel, S. Stoynev, J. Strait, N. Strobbe, L. Taylor, S. Tkaczyk, N.V. Tran, L. Uplegger, E.W. Vaandering, C. Vernieri, M. Verzocchi, R. Vidal, M. Wang, H.A. Weber, A. Whitbeck, W. Wu

University of Florida, Gainesville, USA

D. Acosta, P. Avery, P. Bortignon, D. Bourilkov, A. Brinkerhoff, A. Carnes, M. Carver, D. Curry, R.D. Field, I.K. Furic, S.V. Gleyzer, B.M. Joshi, J. Konigsberg, A. Korytov, K. Kotov, P. Ma, K. Matchev, H. Mei, G. Mitselmakher, K. Shi, D. Sperka, N. Terentyev, L. Thomas, J. Wang, S. Wang, J. Yelton

Florida International University, Miami, USA

Y.R. Joshi, S. Linn, P. Markowitz, J.L. Rodriguez

Florida State University, Tallahassee, USA

A. Ackert, T. Adams, A. Askew, S. Hagopian, V. Hagopian, K.F. Johnson, T. Kolberg, G. Martinez, T. Perry, H. Prosper, A. Saha, A. Santra, V. Sharma, R. Yohay

Florida Institute of Technology, Melbourne, USA

M.M. Baarmand, V. Bhopatkar, S. Colafranceschi, M. Hohlmann, D. Noonan, T. Roy, F. Yumiceva

University of Illinois at Chicago (UIC), Chicago, USA

M.R. Adams, L. Apanasevich, D. Berry, R.R. Betts, R. Cavanaugh, X. Chen, O. Evdokimov, C.E. Gerber, D.A. Hangal, D.J. Hofman, K. Jung, J. Kamin, I.D. Sandoval Gonzalez, M.B. Tonjes, H. Trauger, N. Varelas, H. Wang, Z. Wu, J. Zhang

The University of Iowa, Iowa City, USA

B. Bilki⁶⁴, W. Clarida, K. Dilsiz⁶⁵, S. Durgut, R.P. Gandrajula, M. Haytmyradov, V. Khristenko, J.-P. Merlo, H. Mermerkaya⁶⁶, A. Mestvirishvili, A. Moeller, J. Nachtman, H. Ogul⁶⁷, Y. Onel, F. Ozok⁶⁸, A. Penzo, C. Snyder, E. Tiras, J. Wetzel, K. Yi

Johns Hopkins University, Baltimore, USA

B. Blumenfeld, A. Cocoros, N. Eminizer, D. Fehling, L. Feng, A.V. Gritsan, P. Maksimovic, J. Roskes, U. Sarica, M. Swartz, M. Xiao, C. You

The University of Kansas, Lawrence, USA

A. Al-bataineh, P. Baringer, A. Bean, S. Boren, J. Bowen, J. Castle, S. Khalil, A. Kropivnitskaya, D. Majumder, W. Mcbrayer, M. Murray, C. Rogan, C. Royon, S. Sanders, E. Schmitz, J.D. Tapia Takaki, Q. Wang

Kansas State University, Manhattan, USA

A. Ivanov, K. Kaadze, Y. Maravin, A. Mohammadi, L.K. Saini, N. Skhirtladze

Lawrence Livermore National Laboratory, Livermore, USA

F. Rebassoo, D. Wright

University of Maryland, College Park, USA

A. Baden, O. Baron, A. Belloni, S.C. Eno, Y. Feng, C. Ferraioli, N.J. Hadley, S. Jabeen, G.Y. Jeng, R.G. Kellogg, J. Kunkle, A.C. Mignerey, F. Ricci-Tam, Y.H. Shin, A. Skuja, S.C. Tonwar

Massachusetts Institute of Technology, Cambridge, USA

D. Abercrombie, B. Allen, V. Azzolini, R. Barbieri, A. Baty, G. Bauer, R. Bi, S. Brandt, W. Busza, I.A. Cali, M. D'Alfonso, Z. Demiragli, G. Gomez Ceballos, M. Goncharov, D. Hsu, M. Hu, Y. Iiyama, G.M. Innocenti, M. Klute, D. Kovalskyi, Y.-J. Lee, A. Levin, P.D. Luckey, B. Maier, A.C. Marini, C. Mcginn, C. Mironov, S. Narayanan, X. Niu, C. Paus, C. Roland, G. Roland, J. Salfeld-Nebgen, G.S.F. Stephans, K. Sumorok, K. Tatar, D. Velicanu, J. Wang, T.W. Wang, B. Wyslouch

University of Minnesota, Minneapolis, USA

A.C. Benvenuti, R.M. Chatterjee, A. Evans, P. Hansen, J. Hiltbrand, S. Kalafut, Y. Kubota, Z. Lesko, J. Mans, S. Nourbakhsh, N. Ruckstuhl, R. Rusack, J. Turkewitz, M.A. Wadud

University of Mississippi, Oxford, USA

J.G. Acosta, S. Oliveros

University of Nebraska-Lincoln, Lincoln, USA

E. Avdeeva, K. Bloom, D.R. Claes, C. Fangmeier, F. Golf, R. Gonzalez Suarez, R. Kamalieddin, I. Kravchenko, J. Monroy, J.E. Siado, G.R. Snow, B. Stieger

State University of New York at Buffalo, Buffalo, USA

J. Dolen, A. Godshalk, C. Harrington, I. Iashvili, D. Nguyen, A. Parker, S. Rappoccio, B. Roozbahani

Northeastern University, Boston, USA

G. Alverson, E. Barberis, C. Freer, A. Hortiangtham, A. Massironi, D.M. Morse, T. Orimoto, R. Teixeira De Lima, D. Trocino, T. Wamorkar, B. Wang, A. Wisecarver, D. Wood

Northwestern University, Evanston, USA

S. Bhattacharya, O. Charaf, K.A. Hahn, N. Mucia, N. Odell, M.H. Schmitt, K. Sung, M. Trovato, M. Velasco

University of Notre Dame, Notre Dame, USA

R. Bucci, N. Dev, M. Hildreth, K. Hurtado Anampa, C. Jessop, D.J. Karmgard, N. Kellams, K. Lannon, W. Li, N. Loukas, N. Marinelli, F. Meng, C. Mueller, Y. Musienko³⁶, M. Planer, A. Reinsvold, R. Ruchti, P. Siddireddy, G. Smith, S. Taroni, M. Wayne, A. Wightman, M. Wolf, A. Woodard

The Ohio State University, Columbus, USA

J. Alimena, L. Antonelli, B. Bylsma, L.S. Durkin, S. Flowers, B. Francis, A. Hart, C. Hill, W. Ji, T.Y. Ling, B. Liu, W. Luo, B.L. Winer, H.W. Wulsin

Princeton University, Princeton, USA

S. Cooperstein, O. Driga, P. Elmer, J. Hardenbrook, P. Hebda, S. Higginbotham, A. Kalogeropoulos, D. Lange, J. Luo, D. Marlow, K. Mei, I. Ojalvo, J. Olsen, C. Palmer, P. Piroué, D. Stickland, C. Tully

University of Puerto Rico, Mayaguez, USA

S. Malik, S. Norberg

Purdue University, West Lafayette, USA

A. Barker, V.E. Barnes, S. Das, S. Folgueras, L. Gutay, M. Jones, A.W. Jung, A. Khatiwada, D.H. Miller, N. Neumeister, C.C. Peng, H. Qiu, J.F. Schulte, J. Sun, F. Wang, R. Xiao, W. Xie

Purdue University Northwest, Hammond, USA

T. Cheng, N. Parashar, J. Stupak

Rice University, Houston, USA

Z. Chen, K.M. Ecklund, S. Freed, F.J.M. Geurts, M. Guilbaud, M. Kilpatrick, W. Li, B. Michlin, B.P. Padley, J. Roberts, J. Rorie, W. Shi, Z. Tu, J. Zabel, A. Zhang

University of Rochester, Rochester, USA

A. Bodek, P. de Barbaro, R. Demina, Y.t. Duh, T. Ferbel, M. Galanti, A. Garcia-Bellido, J. Han, O. Hindrichs, A. Khukhunaishvili, K.H. Lo, P. Tan, M. Verzetti

The Rockefeller University, New York, USA

R. Ciesielski, K. Goulianos, C. Mesropian

Rutgers, The State University of New Jersey, Piscataway, USA

A. Agapitos, J.P. Chou, Y. Gershtein, T.A. Gómez Espinosa, E. Halkiadakis, M. Heindl, E. Hughes, S. Kaplan, R. Kunnawalkam Elayavalli, S. Kyriacou, A. Lath, R. Montalvo, K. Nash, M. Osherson, H. Saka, S. Salur, S. Schnetzer, D. Sheffield, S. Somalwar, R. Stone, S. Thomas, P. Thomassen, M. Walker

University of Tennessee, Knoxville, USA

A.G. Delannoy, J. Heideman, G. Riley, K. Rose, S. Spanier, K. Thapa

Texas A&M University, College Station, USA

O. Bouhali⁶⁹, A. Castaneda Hernandez⁶⁹, A. Celik, M. Dalchenko, M. De Mattia, A. Delgado, S. Dildick, R. Eusebi, J. Gilmore, T. Huang, T. Kamon⁷⁰, R. Mueller, Y. Pakhotin, R. Patel, A. Perloff, L. Perniè, D. Rathjens, A. Safonov, A. Tatarinov, K.A. Ulmer

Texas Tech University, Lubbock, USA

N. Akchurin, J. Damgov, F. De Guio, P.R. Duderø, J. Faulkner, E. Gurpinar, S. Kunori, K. Lamichhane, S.W. Lee, T. Libeiro, T. Mengke, S. Muthumuni, T. Peltola, S. Undleeb, I. Volobouev, Z. Wang

Vanderbilt University, Nashville, USA

S. Greene, A. Gurrola, R. Janjam, W. Johns, C. Maguire, A. Melo, H. Ni, K. Padeken, P. Sheldon, S. Tuo, J. Velkovska, Q. Xu

University of Virginia, Charlottesville, USA

M.W. Arenton, P. Barria, B. Cox, R. Hirosky, M. Joyce, A. Ledovskoy, H. Li, C. Neu, T. Sinthuprasith, Y. Wang, E. Wolfe, F. Xia

Wayne State University, Detroit, USA

R. Harr, P.E. Karchin, N. Poudyal, J. Sturdy, P. Thapa, S. Zaleski

University of Wisconsin - Madison, Madison, WI, USA

M. Brodski, J. Buchanan, C. Caillol, D. Carlsmith, S. Dasu, L. Dodd, S. Duric, B. Gomber, M. Grothe, M. Herndon, A. Hervé, U. Hussain, P. Klabbers, A. Lanaro, A. Levine, K. Long, R. Loveless, T. Ruggles, A. Savin, N. Smith, W.H. Smith, D. Taylor, N. Woods

†: Deceased

- 1: Also at Vienna University of Technology, Vienna, Austria
- 2: Also at IRFU, CEA, Université Paris-Saclay, Gif-sur-Yvette, France
- 3: Also at Universidade Estadual de Campinas, Campinas, Brazil
- 4: Also at Federal University of Rio Grande do Sul, Porto Alegre, Brazil
- 5: Also at Université Libre de Bruxelles, Bruxelles, Belgium
- 6: Also at Institute for Theoretical and Experimental Physics, Moscow, Russia
- 7: Also at Joint Institute for Nuclear Research, Dubna, Russia
- 8: Also at Suez University, Suez, Egypt
- 9: Now at British University in Egypt, Cairo, Egypt
- 10: Also at Zewail City of Science and Technology, Zewail, Egypt
- 11: Also at Department of Physics, King Abdulaziz University, Jeddah, Saudi Arabia
- 12: Also at Université de Haute Alsace, Mulhouse, France
- 13: Also at Skobeltsyn Institute of Nuclear Physics, Lomonosov Moscow State University, Moscow, Russia
- 14: Also at Tbilisi State University, Tbilisi, Georgia
- 15: Also at CERN, European Organization for Nuclear Research, Geneva, Switzerland
- 16: Also at RWTH Aachen University, III. Physikalisches Institut A, Aachen, Germany
- 17: Also at University of Hamburg, Hamburg, Germany
- 18: Also at Brandenburg University of Technology, Cottbus, Germany
- 19: Also at MTA-ELTE Lendület CMS Particle and Nuclear Physics Group, Eötvös Loránd University, Budapest, Hungary
- 20: Also at Institute of Nuclear Research ATOMKI, Debrecen, Hungary
- 21: Also at Institute of Physics, University of Debrecen, Debrecen, Hungary
- 22: Also at Indian Institute of Technology Bhubaneswar, Bhubaneswar, India
- 23: Also at Institute of Physics, Bhubaneswar, India
- 24: Also at University of Visva-Bharati, Santiniketan, India
- 25: Also at University of Ruhuna, Matara, Sri Lanka
- 26: Also at Isfahan University of Technology, Isfahan, Iran
- 27: Also at Yazd University, Yazd, Iran
- 28: Also at Plasma Physics Research Center, Science and Research Branch, Islamic Azad University, Tehran, Iran
- 29: Also at Università degli Studi di Siena, Siena, Italy
- 30: Also at INFN Sezione di Milano-Bicocca; Università di Milano-Bicocca, Milano, Italy
- 31: Also at Purdue University, West Lafayette, USA
- 32: Also at International Islamic University of Malaysia, Kuala Lumpur, Malaysia
- 33: Also at Malaysian Nuclear Agency, MOSTI, Kajang, Malaysia
- 34: Also at Consejo Nacional de Ciencia y Tecnología, Mexico city, Mexico
- 35: Also at Warsaw University of Technology, Institute of Electronic Systems, Warsaw, Poland
- 36: Also at Institute for Nuclear Research, Moscow, Russia
- 37: Now at National Research Nuclear University 'Moscow Engineering Physics Institute' (MEPhI), Moscow, Russia

- 38: Also at St. Petersburg State Polytechnical University, St. Petersburg, Russia
- 39: Also at University of Florida, Gainesville, USA
- 40: Also at P.N. Lebedev Physical Institute, Moscow, Russia
- 41: Also at California Institute of Technology, Pasadena, USA
- 42: Also at Budker Institute of Nuclear Physics, Novosibirsk, Russia
- 43: Also at Faculty of Physics, University of Belgrade, Belgrade, Serbia
- 44: Also at University of Belgrade, Faculty of Physics and Vinca Institute of Nuclear Sciences, Belgrade, Serbia
- 45: Also at Scuola Normale e Sezione dell'INFN, Pisa, Italy
- 46: Also at National and Kapodistrian University of Athens, Athens, Greece
- 47: Also at Riga Technical University, Riga, Latvia
- 48: Also at Universität Zürich, Zurich, Switzerland
- 49: Also at Stefan Meyer Institute for Subatomic Physics (SMI), Vienna, Austria
- 50: Also at Adiyaman University, Adiyaman, Turkey
- 51: Also at Istanbul Aydin University, Istanbul, Turkey
- 52: Also at Mersin University, Mersin, Turkey
- 53: Also at Cag University, Mersin, Turkey
- 54: Also at Piri Reis University, Istanbul, Turkey
- 55: Also at Izmir Institute of Technology, Izmir, Turkey
- 56: Also at Necmettin Erbakan University, Konya, Turkey
- 57: Also at Marmara University, Istanbul, Turkey
- 58: Also at Kafkas University, Kars, Turkey
- 59: Also at Istanbul Bilgi University, Istanbul, Turkey
- 60: Also at Rutherford Appleton Laboratory, Didcot, United Kingdom
- 61: Also at School of Physics and Astronomy, University of Southampton, Southampton, United Kingdom
- 62: Also at Instituto de Astrofísica de Canarias, La Laguna, Spain
- 63: Also at Utah Valley University, Orem, USA
- 64: Also at Beykent University, Istanbul, Turkey
- 65: Also at Bingol University, Bingol, Turkey
- 66: Also at Erzincan University, Erzincan, Turkey
- 67: Also at Sinop University, Sinop, Turkey
- 68: Also at Mimar Sinan University, Istanbul, Istanbul, Turkey
- 69: Also at Texas A&M University at Qatar, Doha, Qatar
- 70: Also at Kyungpook National University, Daegu, Korea